Article

Dysregulation of mTOR signalling is a converging mechanism in lissencephaly

https://doi.org/10.1038/s41586-024-08341-9

Received: 20 September 2023

Accepted: 5 November 2024

Published online: 1 January 2025

Open access

Check for updates

Ce Zhang[1,2], Dan Liang[3,29], A. Gulhan Ercan-Sencicek[4,5], Aybike S. Bulut[4,6], Joelly Cortes[4], Iris Q. Cheng[4], Octavian Henegariu[4], Sayoko Nishimura[4], Xinyuan Wang[7], A. Buket Peksen[4], Yutaka Takeo[4], Caner Caglar[4,30], TuKiet T. Lam[8,9], Merve Nur Koroglu[10], Anand Narayanan[11], Francesc Lopez-Giraldez[11], Danielle F. Miyagishima[2,12], Ketu Mishra-Gorur[4], Tanyeri Barak[4,5], Katsuhito Yasuno[4,5], E. Zeynep Erson-Omay[4,13], Cengiz Yalcinkaya[14], Guilin Wang[11,15], Shrikant Mane[11,12], Hande Kaymakcalan[4,16], Aslan Guzel[17,18], A. Okay Caglayan[4,5,19,20], Beyhan Tuysuz[21], Nenad Sestan[3,12,22,23,24], Murat Gunel[3,4,5,11,12,25,26] ✉, Angeliki Louvi[3,4,5] ✉ & Kaya Bilguvar[4,5,6,10,11,12,16,27,28] ✉

Cerebral cortex development in humans is a highly complex and orchestrated process that is under tight genetic regulation. Rare mutations that alter gene expression or function can disrupt the structure of the cerebral cortex, resulting in a range of neurological conditions[1]. Lissencephaly ('smooth brain') spectrum disorders comprise a group of rare, genetically heterogeneous congenital brain malformations commonly associated with epilepsy and intellectual disability[2]. However, the molecular mechanisms underlying disease pathogenesis remain unknown. Here we establish hypoactivity of the mTOR pathway as a clinically relevant molecular mechanism in lissencephaly spectrum disorders. We characterized two types of cerebral organoid derived from individuals with genetically distinct lissencephalies with a recessive mutation in p53-induced death domain protein 1 (*PIDD1*) or a heterozygous chromosome 17p13.3 microdeletion leading to Miller–Dieker lissencephaly syndrome (MDLS). PIDD1-mutant organoids and MDLS organoids recapitulated the thickened cortex typical of human lissencephaly and demonstrated dysregulation of protein translation, metabolism and the mTOR pathway. A brain-selective activator of mTOR complex 1 prevented and reversed cellular and molecular defects in the lissencephaly organoids. Our findings show that a converging molecular mechanism contributes to two genetically distinct lissencephaly spectrum disorders.

Lissencephaly comprises a spectrum of rare structural brain disorders, including agyria, pachygyria and subcortical band heterotopia[1,2], and is characterized by absent or simplified cerebral gyri and thickening of the cortical grey matter[3,4]. The major clinical manifestations include epilepsy and intellectual disability[5]. Our understanding of the underlying cellular events is largely derived from studies of mouse models of natural lissencephaly[6], cell cultures derived from induced pluripotent stem (iPS) cells[7,8] and post-mortem human brains[9], although such samples are not readily accessible. Cerebral organoids derived from individuals with MDLS demonstrate premature neurogenesis and neuronal migration defects[10,11]. However, the molecular mechanisms underlying the pathogenesis of lissencephaly spectrum disorders remain unknown. Recent advances in genome editing, single-cell omics and quantitative proteomics have provided insights into disease pathophysiology.

Using whole-exome sequencing (WES), we discovered recessive mutations in *PIDD1*, which encodes a death-domain-containing protein

[1]Interdepartmental Neuroscience Program, Yale University, New Haven, CT, USA. [2]MD–PhD Program, Yale School of Medicine, New Haven, CT, USA. [3]Department of Neuroscience, Yale School of Medicine, New Haven, CT, USA. [4]Department of Neurosurgery, Yale School of Medicine, New Haven, CT, USA. [5]Yale Program on Neurogenetics, Yale School of Medicine, New Haven, CT, USA. [6]Department of Genome Sciences, Health Sciences Institute, Acibadem University, Istanbul, Turkey. [7]Department of Neurology, Brigham and Women's Hospital and Harvard Medical School, Boston, MA, USA. [8]Keck MS and Proteomics Resource, Yale School of Medicine, New Haven, CT, USA. [9]Department of Molecular Biophysics and Biochemistry, Yale University, New Haven, CT, USA. [10]Department of Biostatistics and Bioinformatics, Health Sciences Institute, Acibadem University, Istanbul, Turkey. [11]Yale Center for Genome Analysis, Yale University, New Haven, CT, USA. [12]Department of Genetics, Yale School of Medicine, New Haven, CT, USA. [13]Department of Biomedical Informatics and Data Science, Yale School of Medicine, New Haven, CT, USA. [14]Department of Neurology, Cerrahpasa Medical School, Istanbul University Cerrahpasa, Istanbul, Turkey. [15]Keck Microarray Shared Resource, Yale School of Medicine, New Haven, CT, USA. [16]Department of Translational Medicine, Health Sciences Institute, Acibadem University, Istanbul, Turkey. [17]Department of Neurosurgery, Faculty of Medicine, Bahcesehir University, Istanbul, Turkey. [18]Department of Neurosurgery, Medical Point Hospital, Gaziantep, Turkey. [19]Department of Medical Genetics, Faculty of Medicine, Dokuz Eylul University, Izmir, Turkey. [20]Department of Molecular Medicine, Institute of Health Sciences, Dokuz Eylul University, Izmir, Turkey. [21]Department of Pediatric Genetics, Cerrahpasa Medical School, Istanbul University Cerrahpasa, Istanbul, Turkey. [22]Department of Comparative Medicine, Yale School of Medicine, New Haven, CT, USA. [23]Department of Psychiatry, Yale School of Medicine, New Haven, CT, USA. [24]Kavli Institute for Neuroscience, Yale School of Medicine, New Haven, CT, USA. [25]Yale Program in Brain Tumor Research, Yale School of Medicine, New Haven, CT, USA. [26]Yale Cancer Center, Yale School of Medicine, New Haven, CT, USA. [27]Department of Medical Genetics, School of Medicine, Acibadem University, Istanbul, Turkey. [28]Rare Diseases and Orphan Drugs Application and Research Center-ACURARE, Acibadem University, Istanbul, Turkey. [29]Present address: Bexorg, Inc., New Haven, CT, USA. [30]Present address: Department of Molecular Biology, Beykoz Institute of Life Sciences and Biotechnology, Bezmialem Vakif University, Istanbul, Turkey. ✉e-mail: murat.gunel@yale.edu; angeliki.louvi@yale.edu; kaya.bilguvar@yale.edu

with unknown function in human brain development, in patients with radiographically established lissencephaly spectrum disorder. Using iPS cell-derived cerebral organoids as a model to recapitulate the first trimester of human cerebrocortical development[12], we integrate cellular, single-cell transcriptomic and proteomic analyses to study disrupted processes that lead to lissencephaly. We show that PIDD1 has a role in the regulation of mTOR signalling during cerebral organoid development and provide evidence of mTOR pathway hypoactivity in PIDD1-mutant organoids and MDLS organoids, thereby implicating a converging molecular mechanism in lissencephaly spectrum disorders.

PIDD1 variants in lissencephaly spectrum disorders

WES identified recessive mutations in *PIDD1* in three unrelated consanguineous families (NG8, NG375 and NG1801) in the Yale Neurogenetics cohort. The three affected members of the NG8 family presented with pachygyria, intellectual disability and arachnoid cysts[13,14] and had a stop-gain mutation (W589X). In families NG375 and NG1801, three individuals with diffuse pachygyria and intellectual disability also had stop-gain (R331X) or splice-site (c.2042-2A>G) mutations in *PIDD1* (Extended Data Figs. 1a–d and 2a–c, Supplementary Tables 1 and 2 and Methods). Constitutive autoproteolysis of PIDD1 generates an amino-terminal fragment with an uncharacterized regulatory role and two carboxy-terminal fragments, PIDD1-C and PIDD1-CC. These two fragments operate as molecular switches through differential binding to RIP1 and NEMO (PIDD1-C), to trigger NF-κB pro-survival signalling pathways, or to CRADD and CASP2 (PIDD1-CC), to activate pro-apoptotic responses[15] (Extended Data Fig. 1e,f). The mutations are predicted to lead to complete (stop-gain) or partial (splice-site) loss of PIDD1-CC, which includes the death domain (Extended Data Fig. 1e,g), thereby disrupting the CASP2-PIDDosome. Supporting these findings, biallelic mutations in *PIDD1*, *CRADD* or *CASP2* were recently reported in families with lissencephaly spectrum disorders and intellectual disability[16–21].

Progenitor defects in mutant organoids

Hair follicle keratinocytes from an individual with a homozygous R331X mutation were reprogrammed to iPS cells (Extended Data Fig. 3a). The patient-derived cell line (patient) and an outside-family cell line (control) were deemed pluripotent through teratoma assays (Extended Data Fig. 3b) and through assessment of OCT4 and NANOG expression (Extended Data Fig. 3c). CRISPR–Cas9 gene editing was used to generate an isogenic 'rescue' cell line and a 'knock-in' cell line. For the rescue cell line, both mutant alleles of the patient cell line were corrected to the wild-type allele, whereas for the knock-in cell line, two mutant alleles were introduced into the control cell line (Extended Data Fig. 3d,e, Supplementary Fig. 2 and Methods). The control, patient, knock-in and rescue iPS cells had normal karyotype and gave rise to dorsal forebrain organoids (Extended Data Fig. 3d,f,g and Methods). The organoids had ventricular zone (VZ)-like, subventricular zone (SVZ)-like and cortical plate (CP)-like layers, thereby resembling early fetal cortical development (Extended Data Fig. 3h). In contrast to the control and rescue counterparts, patient organoids and knock-in organoids did not express the PIDD1-CC fragment (Extended Data Fig. 3i). These results demonstrate that these four iPS cell lines exhibit a stable and expected genomic and PIDD1 expression profile.

Control, patient, knock-in and rescue organoids were grown and analysed at day 50 (D50) and D70. Cleaved caspase-3-positive ($CC3^+$) neural progenitors in the VZ-like and SVZ-like areas were reduced in patient and knock-in organoids (Fig. 1a,b and Extended Data Fig. 4a,b), a result consistent with a lack of the PIDD1-CC fragment necessary to activate caspase-2 and cell death[17] (Extended Data Fig. 1e,f). In the SVZ, where basal progenitors reside, we detected a decrease in $HOPX^+$ outer radial glia (oRG) cells at D50 and D70 (Fig. 1c,d and Extended Data Fig. 4c,d), but no differences in $TBR2^+$ intermediate progenitor cells (IPCs) at D70 (Extended Data Fig. 4e,f); the latter showed reduced numbers of $CC3^+$ cells (Extended Data Fig. 4g–i). No significant differences were seen in the number of EdU-incorporating S phase cells and $MKI67^+$ proliferating cells in the VZ and SVZ at D50 (Extended Data Fig. 5a,b), or $SOX2^+$ progenitors in the SVZ at D70 (Fig. 1e). Together, these findings demonstrate that PIDD1-mutant organoids have reduced numbers of $HOPX^+$ oRG progenitors, an effect that is not attributable to changes in cell proliferation or cell death.

Neural progenitors in the organoid VZ undergo symmetric proliferative divisions with vertical cleavage planes (60–90° relative to the ventricular surface) and asymmetric neurogenic divisions with horizontal (0–30°) or oblique (30–60°) cleavage planes[22]. We observed no differences in the number of phosphorylated histone H3-positive ($PH3^+$) mitotic progenitor cells lining the apical surface of the VZ among genotypes at D50 (Extended Data Fig. 5c,d), a result consistent with unperturbed proliferation. However, patient and knock-in organoids had more VZ cells undergoing asymmetric division (Extended Data Fig. 5e,f), fewer $SOX2^+$ progenitors and more $MAP2^+$ neurons (Extended Data Fig. 5g,h), a result suggestive of an increased neurogenic state in PIDD1-mutant progenitors.

CP abnormalities in mutant organoids

Thickening of the cerebral cortex is a key feature of lissencephaly spectrum disorders and a consistent radiographical finding in patients with *PIDD1* mutations[17,18] (Extended Data Fig. 2a–c). We investigated laminar cytoarchitecture by immunostaining with markers of deep (CTIP2) and upper (SATB2) layer neurons (Fig. 2a and Extended Data Fig. 6a,c). We observed a marked increase in the relative thickness of the CP in patient and knock-in organoids at D50 and D70 (Fig. 2a,b and Extended Data Fig. 6a,b), a result reminiscent of the thickened cortex characteristic of human lissencephaly. In the CP, SATB2 was co-localized with CTIP2 at D50 (Extended Data Fig. 6d), whereas at D70, we identified $CTIP2^+SATB2^+$, $SATB2^+$ and $CTIP2^+$ neuronal populations. Notably, patient and knock-in organoids had more double-positive and fewer single-positive ($SATB2^+$ or $CTIP2^+$) cells compared with control and rescue counterparts (Extended Data Fig. 6e,f), a result suggesting that neuronal differentiation is defective. At D120, $SATB2^+$ cells were broadly distributed (Fig. 2c,d) and at an increased density (Fig. 2e), indicative of increased production in patient and knock-in organoids; this led to continued abnormal expansion of the CP. Golgi–Cox staining of D120 organoids did not reveal any obvious defects in neuronal morphology (Extended Data Fig. 6g). Altogether, these results indicate that PIDD1-mutant organoids display a persistent thickened CP-like area, defective cortical lamination and impaired neural differentiation.

Dysregulation in the transcriptome

To examine transcriptional perturbations and associated cellular states, we performed single-cell RNA sequencing (scRNA-seq) in control, patient, knock-in and rescue organoids at D70. We analysed 151,506 cells, which formed 10 distinct and well-annotated uniform manifold approximation and projection (UMAP) clusters (Fig. 3a,b and Methods). We also performed gene ontology (GO) biological pathway enrichment analysis using three comparisons (patient versus control, knock-in versus control, and patient versus rescue) in the radial glia (RG), oRG, IPC and dividing IPC clusters. In the oRG and both IPC clusters, common downregulated GO terms included generation of neurons, neuron differentiation, neuron projection development and neuron development. Notably, common upregulated GO terms were related to protein metabolism, including translation, peptide-related processes, amide-related processes and ribonucleoprotein complex biogenesis (Fig. 3c). *PIDD1* expression was highly enriched in neural progenitor cell clusters in control and patient organoids and reduced

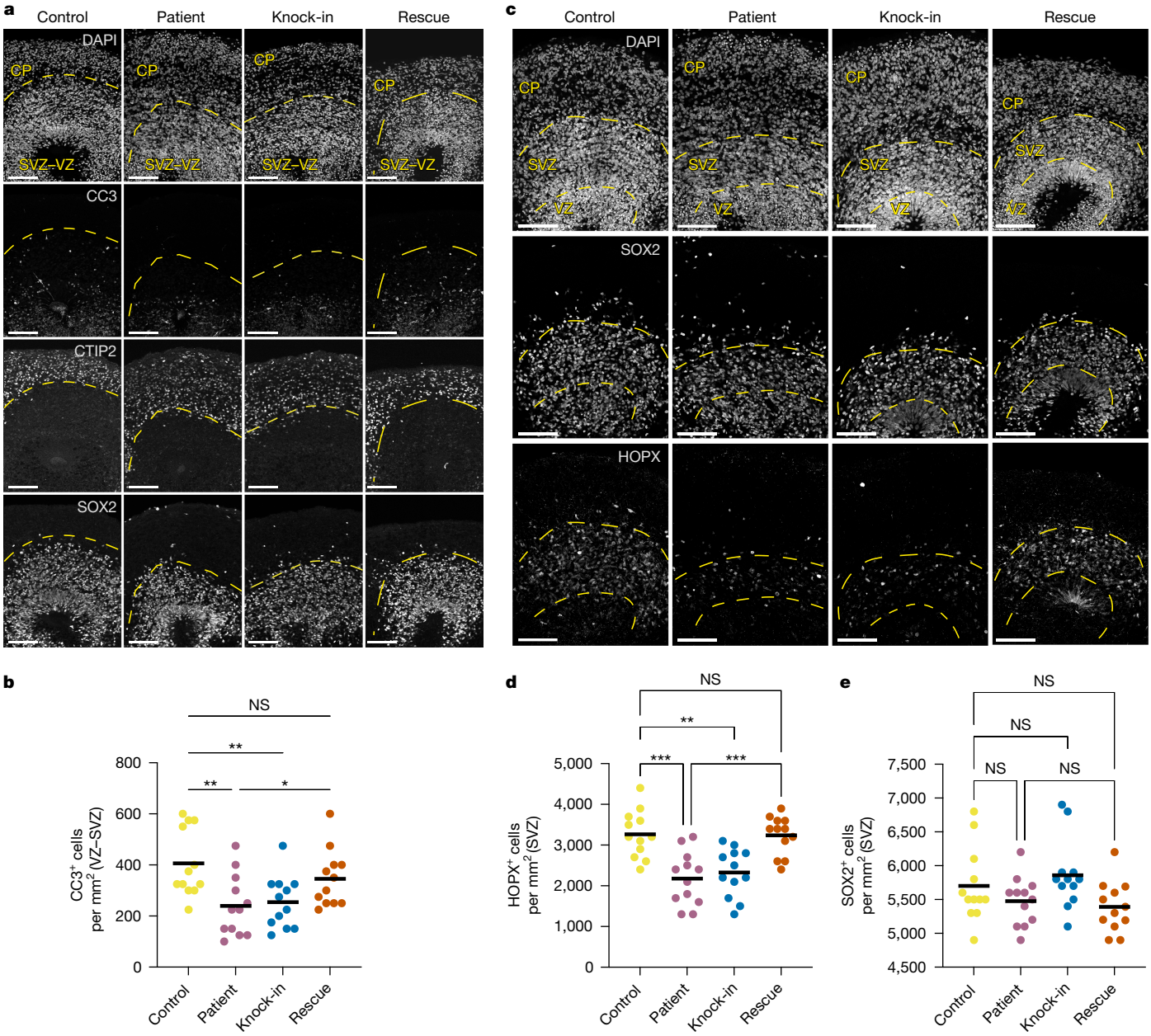

Fig. 1 | Neural progenitor dysregulation in PIDD1-mutant organoids. **a**, Control, patient, knock-in and rescue organoids at D70 immunostained for CC3, CTIP2 and SOX2. Yellow dashed lines delineate the CP, the SVZ and the VZ. **b**, Quantification of $CC3^+$ cells per mm^2 of the SVZ–VZ area. **c**, Control, patient, knock-in and rescue organoids at D70 immunostained for SOX2 (neural progenitor cells) and HOPX (oRG cells). **d**,**e**, Quantification of $HOPX^+$ (**d**) and $SOX2^+$ (**e**) cells per mm^2 of the SVZ area. All analyses were performed using images from $n = 12$ cortical regions, $n = 6$ organoids, 2 batches of 3 organoids per genotype. Statistical test: one-way analysis of variance (ANOVA). $^{***}P < 0.001$, $^{**}P < 0.01$, $^{*}P < 0.05$. NS, not significant. Scale bars, 100 µm.

in the latter (Fig. 3d). We used quantitative PCR with reverse transcription (RT–qPCR) in D70 organoids treated with 50 µM cycloheximide, an inhibitor of nonsense-mediated decay, to confirm that the decrease in *PIDD1* expression in patient organoids is consistent with nonsense-mediated decay (Extended Data Fig. 1h). Average expression was lower in excitatory neuron clusters than in progenitor clusters, a result consistent with a previous scRNA-seq analysis of the developing mouse brain[23]. *PIDD1* is expressed throughout human brain development[24] (Extended Data Fig. 7a), including in the VZ, the SVZ and the CP of gestational week 17 human fetal cortex and in the VZ-like and SVZ-like progenitor areas of D70 organoids (Extended Data Fig. 7b,c). Next, we analysed the scRNA-seq data for pathways enriched in *PIDD1*-expressing cells compared with non-expressing cells in control and patient organoids in pseudobulk (mixed-cell) samples (Fig. 3e and Extended Data Fig. 7d). GO enrichment analysis for biological processes comparing *PIDD1*-expressing cells with non-expressing cells in control organoids demonstrated upregulation in stress and hypoxia responses and cell death pathways (Extended Data Fig. 7d), a result consistent with known PIDD1 functions[25,26]. Downregulated processes included neurogenesis and neuron differentiation, which suggests that *PIDD1* expression might be important for maintaining a non-neuronal state. We also compared *PIDD1*-expressing cells in patient and control organoids to determine the impact of this mutation on biological processes (Fig. 3e). Metabolic processes and translation ontologies were upregulated in *PIDD1*-expressing cells in patient organoids, whereas generation of neurons was downregulated, similar to the *PIDD1*-expressing progenitor cell clusters in patient and knock-in organoids. Notably, lissencephaly was the second most

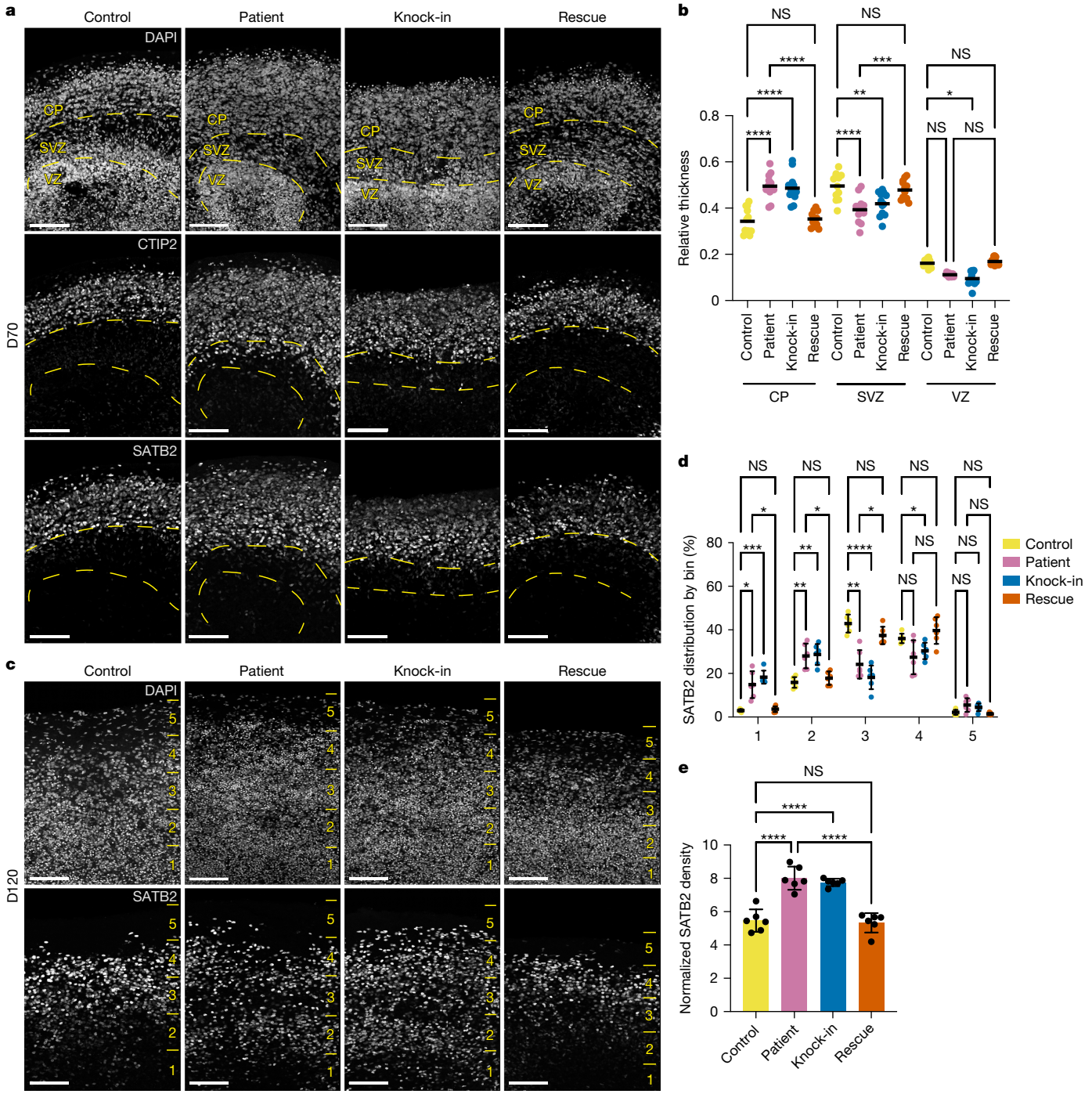

Fig. 2 | CP defects in PIDD1-mutant organoids. a, Control, patient, knock-in and rescue organoids at D70 immunostained for CTIP2 and SATB2 (deep and upper, respectively, cortical layer neurons). Yellow dashed lines delineate the CP, the SVZ and the VZ. **b**, Quantification of the relative thickness of the VZ, the SVZ and the CP from **a**. **c**, Control, patient, knock-in and rescue organoids at D120 immunostained for SATB2. **d**, Quantification of the distribution of SATB2-expressing cells across five equal bins shown in **c**. **e**, Quantification of the normalized density of SATB2-expressing cells from the organoid surface to the bottom of the images in **c**. $n = 12$ cortical regions, $n = 6$ organoids, 2 batches of 3 organoids per genotype (**b**); $n = 6$ cortical regions, $n = 6$ organoids, 2 batches of 3 organoids per genotype (**d**,**e**). Statistical tests: one-way ANOVA (**b**,**e**) or two-way ANOVA (**d**). $^{****}P < 0.0001$, $^{***}P < 0.001$, $^{**}P < 0.01$, $^{*}P < 0.05$. Data are mean ± s.d. (**d**,**e**). Scale bars, 100 µm.

significant disease process enriched for differentially expressed genes (DEGs) that were downregulated in *PIDD1*-expressing cells in patient organoids compared with control organoids (using an OMIM dataset of known human disease-causing genes; Extended Data Fig. 7e). Overall, analyses of scRNA-seq data demonstrate that disruption of PIDD1 may lead to dysregulation of translational, metabolic and neurogenic pathways.

In the human brain, mTOR signalling is a key regulator of protein translation and development of neural progenitors, including oRG cells[27,28]. The expression of many mTOR pathway genes was dysregulated in patient and knock-in organoids (Fig. 3f), and was either directly or inversely correlated with *PIDD1* expression in organoids of all genotypes (Fig. 3g). These results imply that *PIDD1* mutation leads to mTOR pathway dysregulation and subsequent perturbation of protein translation and metabolism.

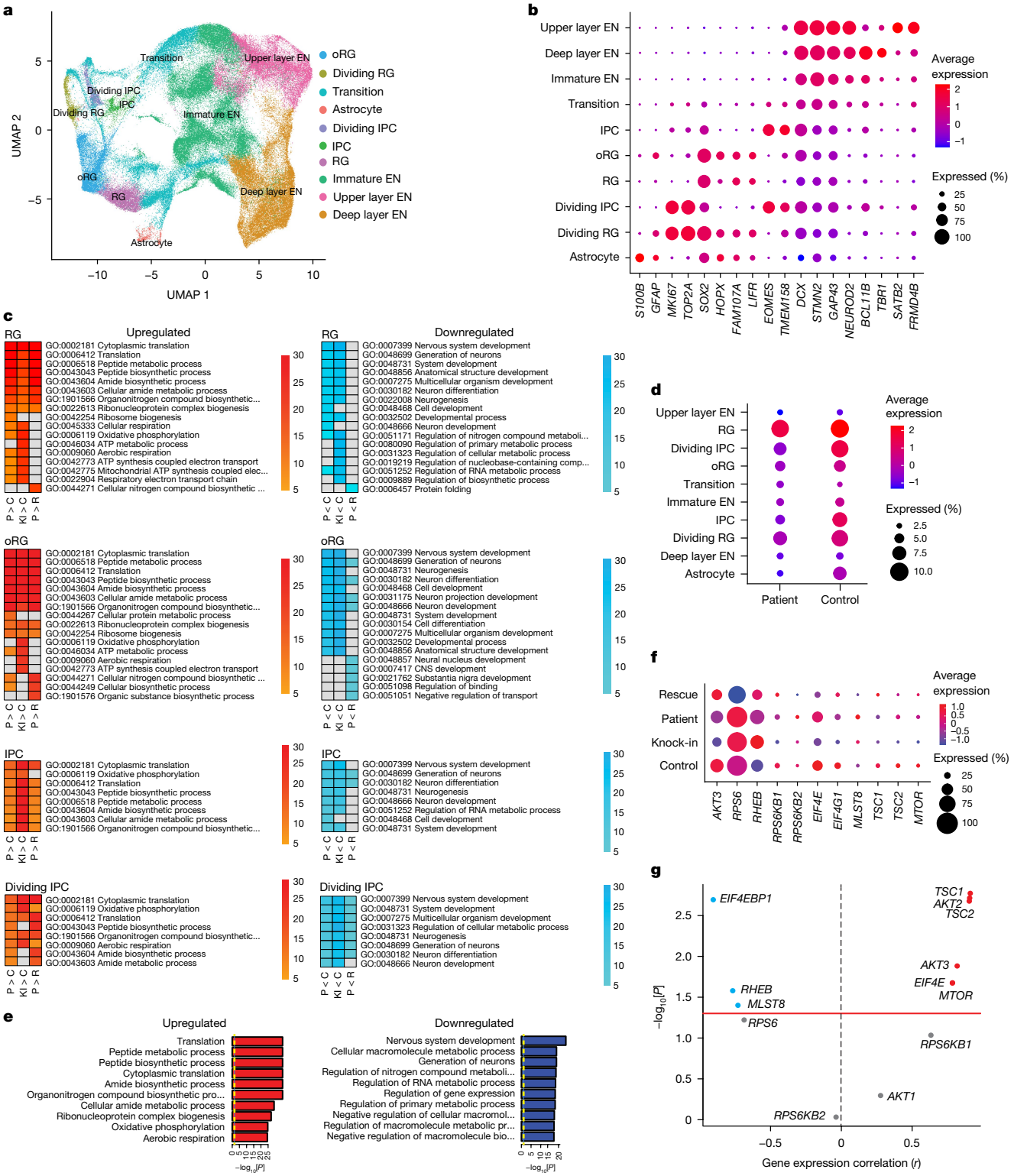

Fig. 3 | scRNA-seq reveals transcriptional dysregulation in PIDD1-mutant organoids. a, UMAP projection of all cells from scRNA-seq of control, patient, knock-in and rescue organoids at D70. EN, excitatory neuron; transition, transitional cell between the progenitor and neuronal state. **b**, Dot plot of the expression of selected established marker genes used for cell-type classification of the entire dataset. **c**, Heat maps representing $-\log_{10}$(adjusted *P* value) of enriched GO terms in RG, oRG, IPC and dividing IPC clusters across three conditions: patient versus control (P > C), knock-in versus control (KI > C), and patient versus rescue (P > R). Left and right heat maps display upregulated and downregulated GO terms, respectively. The top 17 significant GO terms for RG and oRG are plotted for each comparison. Selected GO terms from RG and oRG lists were plotted for IPC and dividing IPC clusters. Grey boxes indicate GO terms that were not significantly upregulated or downregulated for the comparison. **d**, Dot plot of *PIDD1* expression in different cell clusters. **e**, Bar graphs of upregulated (left) and downregulated (right) GO pathways for *PIDD1*-expressing cells in patient organoids ($n = 4$) compared with control organoids ($n = 4$). **f**, Dot plot of the expression of mTOR pathway genes in control, patient, knock-in and rescue whole organoids (pseudobulk analysis). **g**, Gene expression correlation (*r*) of *PIDD1* and mTOR pathway genes across all organoid genotypes (all clusters). Statistical tests: two-tailed Fisher's exact test (**e**) or Pearson's correlation test (**g**) with a *P* value threshold of <0.05. Number of organoids analysed by scRNA-seq: control, $n = 4$; patient, $n = 4$; knock-in, $n = 2$, rescue, $n = 2$.

Dysregulation in the proteome

To evaluate changes at the protein level, we performed high-resolution liquid chromatography with tandem mass spectrometry (LC–MS/MS) in patient and control organoids at D70 (Extended Data Fig. 8a). Pathway enrichment analysis using the MSigDB 2020 Hallmark gene set with gene set enrichment analysis (GSEA; https://www.gsea-msigdb.org/gsea/index.jsp) indicated mTOR complex 1 (mTORC1) signalling as one of the top three downregulated pathways (Extended Data Fig. 8a,b). mTORC1 is a key mTOR pathway component that controls protein translation and ribosome biogenesis[29]. Notably, enriched GO terms of downregulated proteins in patient organoids compared with control organoids included translation, ribosome biogenesis and peptide-related processes (Extended Data Fig. 8c). However, these were found to be upregulated in the corresponding scRNA-seq datasets (Fig. 3c), which suggests that transcriptional upregulation might be a compensatory response to protein downregulation. Furthermore, 848 DEGs in patient and control oRG cells (the progenitor cell type predominantly affected in patient organoids; Fig. 1c,d) overlapped with differentially expressed proteins (DEPs) in patient and control organoids. MSigDB pathway analysis of overlapping DEGs and DEPs in patient and control organoids also included mTORC1 signalling among the top three downregulated pathways (Extended Data Fig. 8d). Together, these analyses provide mutually supportive evidence that PIDD1 dysfunction leads to dysregulation of mTOR signalling at the transcriptomic and proteomic levels.

Increased horizontal divisions and premature neurogenesis are common features of PIDD1-mutant organoids (Fig. 2 and Extended Data Figs. 5e–h and 6a,b) and MDLS[10,11] organoids, which suggests that they share an underlying molecular mechanism. We obtained and validated an MDLS iPS cell line (Extended Data Fig. 3j,k and Methods) and repeated LC–MS/MS to include control, patient, knock-in and MDLS organoids at D70 (Fig. 4a–f). We identified DEPs (Fig. 4a,c,e) and performed pathway analysis comparing patient, knock-in and MDLS organoids to control organoids (Fig. 4b,d,f). mTORC1 signalling was a downregulated pathway enriched in all three comparisons. Overall, 522 DEGs in knock-in oRG cells compared with control oRG cells overlapped with DEPs in knock-in organoids compared with control organoids (Extended Data Fig. 8e). MSigDB pathway analysis of overlapping DEGs and DEPs included mTORC1 signalling among the top three downregulated pathways. Consistent with this and earlier analyses (Extended Data Fig. 8d), mTORC1 signalling was among the top five downregulated pathways in overlapping DEGs and DEPs in patient organoids compared with control organoids (Extended Data Fig. 8f). We also found lower mean protein expression in patient, knock-in and MDLS organoids compared with control organoids (patient versus control, $P = 0.0003$; knock-in versus control, $P < 0.0001$; MDLS versus control, $P = 0.0021$) (Fig. 4g). This result suggests that PIDD1-mutant and MDLS organoids exhibit decreased translation. Last, we identified downregulated DEPs shared between knock-in and MDLS organoids compared with control organoids and between patient and MDLS organoids compared with control organoids and performed GO enrichment analyses for biological processes. Translation and ribosome biogenesis were significantly enriched in both comparisons, which indicates that downregulated translation and ribosome biogenesis are convergent dysregulated mechanisms in PIDD1-mutant organoids and MDLS organoids (Fig. 4h). Altogether, these proteomic analyses indicate a decreased mTORC1 signalling signature shared between MDLS organoids and PIDD1-mutant organoids.

Hypoactivation of mTOR signalling

Next, we sought orthogonal evidence to show that mTOR signalling is decreased in PIDD1-mutant organoids and MDLS organoids. Phosphorylation of the ribosomal protein S6 (pS6) is an indicator of mTORC1 activation, which promotes protein translation[30]. In the organoid SVZ, pS6 was primarily expressed in oRG cells and in a small proportion of IPCs (Extended Data Fig. 9a–c). Consistent with transcriptional dysregulation of mTOR pathway genes in PIDD1-mutant organoids (Fig. 3g), $pS6^{+}SOX2^{+}$ cells and/or relative pS6 signal intensities in the SVZ of patient, knock-in (Extended Data Fig. 9d–f) and MDLS organoids (Fig. 5a,b) and protein levels of phosphorylated AKT (pAKT) and pS6 (Fig. 5c–e) were significantly reduced compared with control and rescue counterparts. These results support the transcriptomic and proteomic findings and identify hypoactive mTOR signalling as a shared molecular mechanism in two lissencephaly spectrum disorders with distinct genetic causes.

Pharmacological rescue of cellular phenotypes

There are currently no viable therapeutic strategies for the prevention or treatment of lissencephaly. Drugs that inhibit mTOR pathway hyperactivity have proven effective for a range of clinical indications[31]. We treated control, patient, knock-in and MDLS organoids with NV-5138 (50 μM), an oral, brain-selective and highly specific mTORC1 activator[32,33] currently in phase II clinical trials for treatment-resistant depression[34], beginning at D30, a time point when neurons emerge[22] (Fig. 6a). NV-5138 acts by directly binding to sestrin-2 and facilitating its dissociation from GATOR2, which in turn leads to mTORC1 activation[32] (Fig. 6b). Immunostaining at D70 demonstrated that the intensity of pS6 was higher in the SVZ of NV-5138-treated organoids than in non-treated organoids, thereby confirming a robust increase in mTORC1 signalling in the former (Fig. 6c). Like their patient and knock-in counterparts, MDLS organoids displayed a thickened CP, a result consistent with premature neurogenesis[10,11]. Sustained application of NV-5138 prevented CP expansion in PIDD1-mutant organoids and in MDLS organoids at D70 (Fig. 6d and Extended Data Fig. 10a). Next, we asked whether it was possible to reverse CP defects and applied NV-5138 at D50 (Fig. 6e), when a thickened CP is already present (Extended Data Fig. 6a,b). At D70, patient and knock-in (and MDLS) organoids displayed reduced pS6 intensities in the CP (Fig. 6f), as in the SVZ (Fig. 5b). Delayed onset of drug application resulted in increased pS6 intensity in the CP (Fig. 6g) and reversed abnormal neuronal distribution in the CP of patient and knock-in organoids at D120 (Fig. 6h). These findings suggest that hypoactive mTORC1 signalling leads to cortical lamination defects in PIDD1-mutant organoids.

We also assessed the effect of NV-5138-mediated mTORC1 activation in oRG cells, which have active mTOR signalling[28] and are affected in PIDD1-mutant organoids (this study) and in MDLS[11] organoids (Extended Data Fig. 10b). NV-5138 application beginning at D30 led to robust increases in the $HOPX^{+}$ oRG population in patient organoids and MDLS organoids at D70 (Extended Data Fig. 10c). The mean pS6 intensity per $HOPX^{+}$ cell was lower in patient and MDLS organoids than in control organoids and increased significantly after NV-5138 treatment (Extended Data Fig. 10d). Altogether, these results demonstrate that NV-5138-meditated mTORC1 activation in PIDD1-mutant organoids and MDLS organoids can rescue the $HOPX^{+}$ oRG population and increase mTOR signalling in these cells.

Next, we performed scRNA-seq of untreated and NV-5138-treated (D30–D100) control, patient and MDLS organoids (136,807 cells) (Extended Data Fig. 10e,f). NV-5138 directly increased the average expression of genes involved in translation, ribosome and ribonucleoprotein complex biogenesis, metabolism and mTOR signalling pathways, and reduced the average expression of neuron-related pathways in the RG and/or oRG clusters across control, patient and MDLS organoids (Extended Data Fig. 10g,h). This result is in line with our intended use of this compound to promote mTOR signalling and reduce premature neurogenesis. Gene expression of translation, metabolic or mTOR signalling pathways remained persistently upregulated in patient organoids and MDLS organoids despite drug treatment

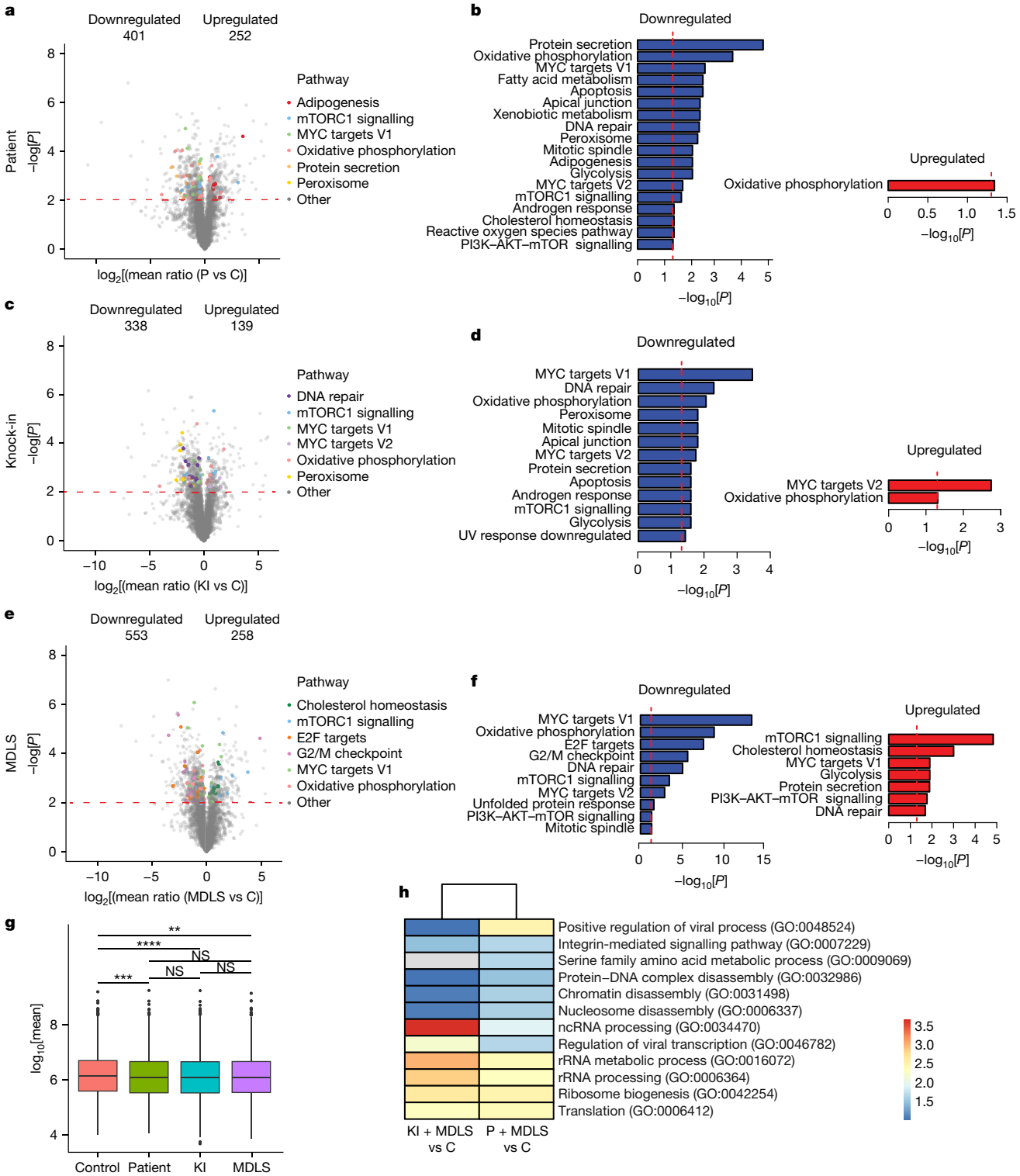

Fig. 4 | MS analyses reveal dysregulated protein pathways in PIDD1-mutant and MDLS organoids. **a**,**b**, Volcano plot of DEPs and selected pathways (**a**) and pathway enrichment (PE) analysis (**b**) for patient organoids versus control organoids at D70; bar graphs of downregulated (left) and upregulated (right) pathways in patient organoids. **c**,**d**, Volcano plot of DEPs and selected pathways (**c**) and PE analysis (**d**) for knock-in organoids versus control organoids at D70; bar graphs of downregulated (left) and upregulated (right) pathways in knock-in organoids. **e**,**f**, Volcano plot of DEPs and selected pathways (**e**) and PE analysis (**f**) for MDLS organoids versus control organoids at D70; bar graphs of downregulated (left) and upregulated (right) pathways in MDLS organoids. **g**, Mean protein translation in MS datasets. Box and whisker plots represent 25th to 75th percentiles of the data, with the centre line representing the median and whiskers representing minima and maxima. Two-tailed paired *t*-test. ****$P < 0.0001$, ***$P < 0.001$, **$P < 0.01$. **h**, Heat maps of selected enriched GO terms in knock-in organoids and MDLS organoids versus control organoids (left) and patient organoids and MDLS organoids versus control organoids (right). Colour bar represents −log(adjusted *P* value). In **a**,**c**,**e**, a two-tailed ANOVA was used. In **b**,**d**,**f**, the MSigDB 2020 Hallmark gene set from GSEA was used in pathway analysis and a two-tailed Fisher's exact test was used. Pathways appearing as both upregulated and downregulated in the bioinformatic analysis indicate that different pathway genes are upregulated or downregulated. Number of organoid replicates for all analyses for MS: control, $n = 3$; patient, $n = 3$; knock-in, $n = 3$; MDLS, $n = 3$; each replicate was a mixture of 3 organoids. *P* value threshold: $P = 0.01$ (**a**,**c**,**e**) or $P = 0.05$ (**b**,**d**,**f**–**h**).

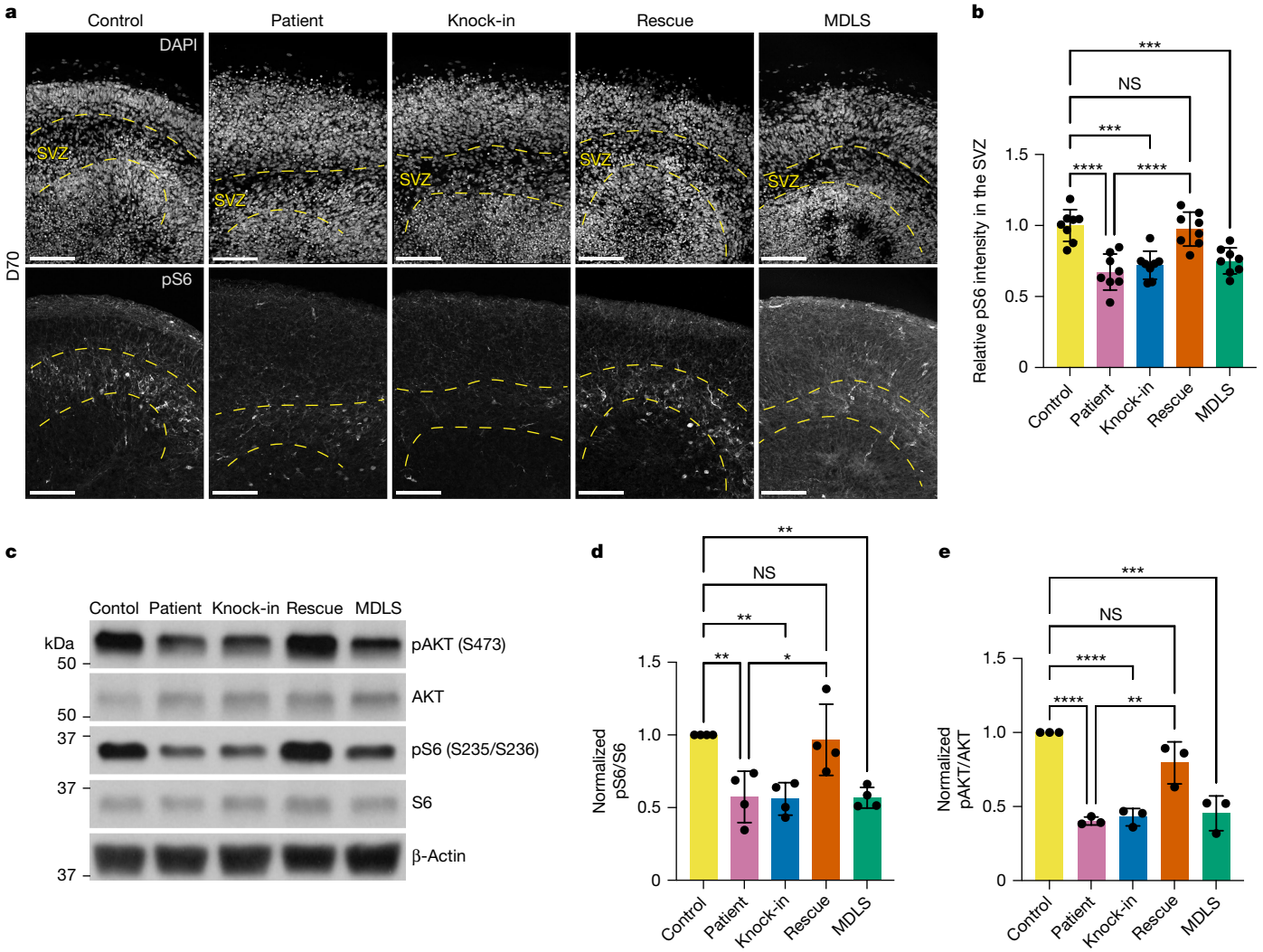

Fig. 5 | Hypoactive mTOR signalling in PIDD1-mutant organoids and MDLS organoids. a, Control, patient, knock-in, rescue and MDLS organoids at D70 immunostained for pS6. Yellow dashed lines delineate the SVZ. **b**, Quantification of pS6 relative intensity in the SVZ area. **c**, Representative western blot of organoid lysates for mTOR pathway components. For gel source data, see Supplementary Fig. 1a. **d**,**e**, Quantification of band intensity for pS6/S6 (**d**) and pAKT(S473)/AKT (**e**) ratios normalized to control. For western blots, $n = 4$ independent batches for pS6/S6, $n = 3$ independent batches for pAKT/AKT, 3 organoids collected per batch per genotype. Analyses of immunostaining experiments were performed with images from $n = 8$ cortical regions, $n = 4$ organoids, 2 batches of 2 organoids per genotype. Statistical test: one-way ANOVA. $^{****}P < 0.0001$, $^{***}P < 0.001$, $^{**}P < 0.01$, $^{*}P < 0.05$. Data are the mean ± s.d. (**b**–**e**). Scale bars, 100 µm.

(Extended Data Fig. 10i), which suggests that reversal of transcriptomic defects is not required for the rescue of organoid phenotypes. These observations suggest that a brain-selective mTORC1-activating small molecule (Fig. 6c,g) can prevent or reverse morphological and functional defects in organoids derived from patients with distinct lissencephaly spectrum subtypes.

Discussion

In this study, using transcriptomic, proteomic and pharmacological approaches in patient-derived organoids, we implicate dysregulated mTOR signalling as a converging molecular mechanism contributing to two genetically distinct lissencephaly spectrum disorders. mTOR signalling is crucial for human cortical development[35]. Mosaic and germline mutations in mTOR regulatory genes that lead to pathway hyperactivation have been associated with focal 'mTORopathies', for example, hemimegalencephaly, polymicrogyria (increased gyration), focal cortical dysplasia and tuberous sclerosis[36–41]. Increased neural progenitor proliferation, oRG expansion and delayed neuronal differentiation are common features of organoids with hyperactive mTOR signalling[36,42,43], which probably favours expansion of the progenitor pool at the expense of neurogenesis. By contrast, PIDD1-mutant organoids and MDLS organoids with hypoactive mTOR signalling displayed increased neurogenesis and CP expansion. Thus, normal PIDD1 function in the cerebral cortex may be important for maintaining progenitor or non-neuronal states through normally operating mTOR signalling. One potential mechanism for this effect is that mTORC1 affects neuronal differentiation through translational control[44]. Indeed, we found evidence of transcriptional dysregulation of translation and ribosome biogenesis and decreased translation in lissencephaly organoids. A mechanical simulation model of human cortical folding[45] suggested that increased CP thickness may result in pachygyria or agyria. Thus, attenuating pathological expansion of the CP by restoring normal mTORC1 activity may represent a downstream mechanism for preventing or reversing decreased gyrification and sulcation in lissencephaly spectrum disorders.

Our study has several limitations. At the stages analysed, organoids lack cell types important for human cortical development and

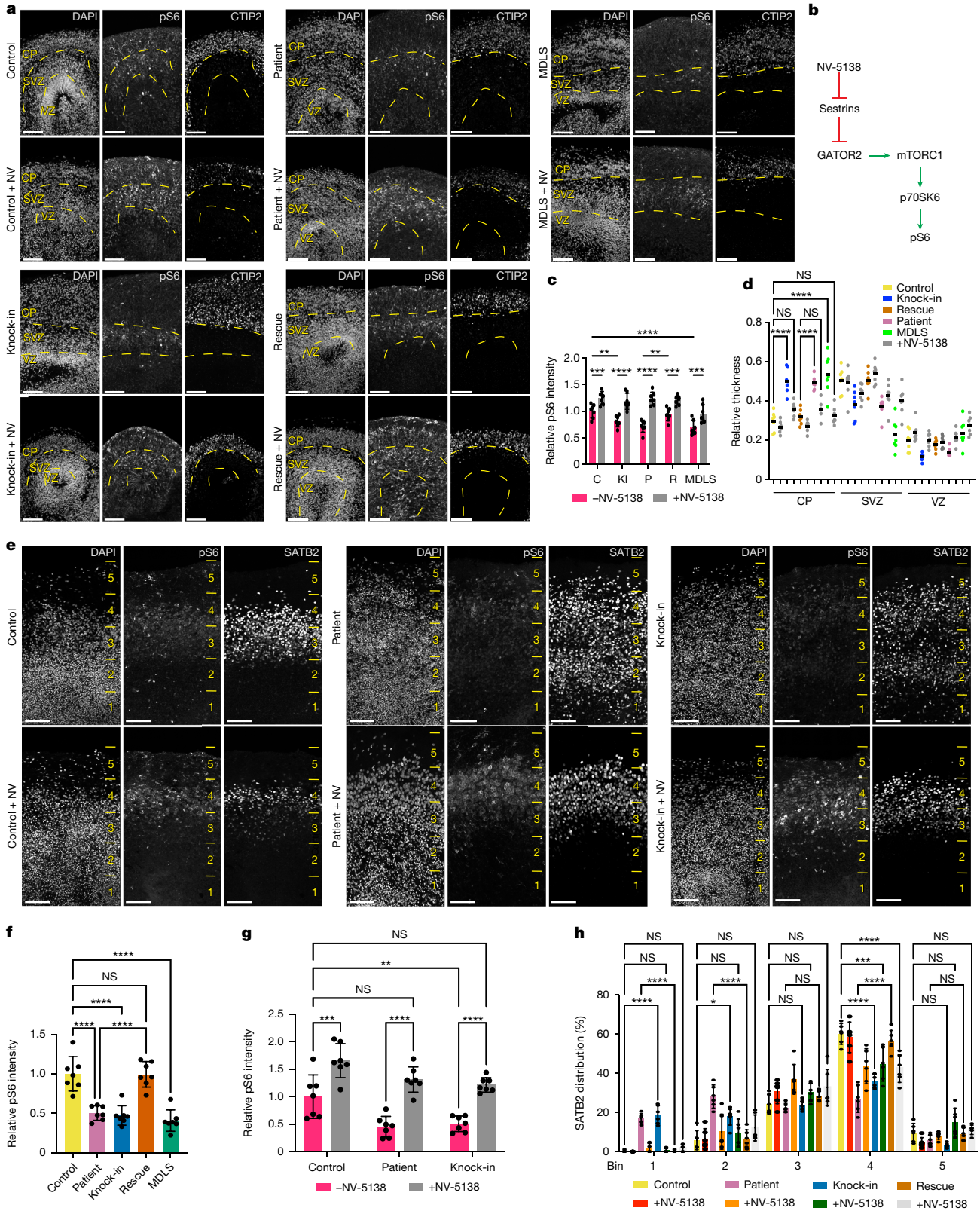

Fig. 6 | An mTORC1 activator rescues mTOR pathway hypoactivity and thickened CP in PIDD1-mutant organoids and MDLS organoids. a, Control, patient, MDLS, knock-in and rescue organoids at D70 grown with or without NV-5138 (NV) starting at D30 immunostained for pS6 and CTIP2. Yellow dashed lines delineate the CP, the SVZ and the VZ. **b**, Diagram illustrating the action of NV-5138 on the mTORC1 pathway. **c**, Quantification of the relative pS6 signal intensity in the SVZ area of D70 organoids. **d**, Quantification of the relative thickness of the CP, the SVZ and the VZ in D70 organoids. **e**, Control, patient and knock-in organoids at D120 grown with or without NV-5138 starting at D50 immunostained for pS6 and SATB2. **f**, Quantification of the relative pS6 signal intensity in the CP area of D70 organoids. **g**, Quantification of the relative pS6 signal intensity in the CP area of D120 organoids. **h**, Quantification of the distribution of SATB2-expressing cells across 5 equal bins of the CP area in D120 organoids shown in **e**. $n = 7$ cortical regions, $n = 6$ organoids, 2 batches per genotype (**c**,**d**,**f**,**g**); $n = 6$ cortical regions, $n = 6$ organoids, 2 batches per genotype (**h**). Statistical tests: one-way ANOVA (**c**,**d**,**f**,) or two-way ANOVA (**g**,**h**). $^{****}P < 0.0001$, $^{***}P < 0.001$, $^{**}P < 0.01$, $^{*}P < 0.05$. Data are the mean ± s.d. (**c**,**f**–**h**). Scale bars, 100 µm.

maturation, including microglia[46] and interneurons[47] and distinct RG subtypes[48]. The lack of post-mortem brain tissue from patients with *PIDD1* mutations prevents us from validating the observations obtained using organoids. In addition to evaluating mTOR signalling in other lissencephaly spectrum disorders, it will be important to develop organoid models with a mature CP that can undergo gyrification to unequivocally link our findings to cortical folding. Finally, aberrant mTOR activation may lead to mTORopathies[41], which represents a concern with the clinical use of mTORC1 activators. It will be essential to investigate whether correcting mTOR hypoactivation may be a therapeutic option worth exploring in lissencephaly spectrum disorders.

In conclusion, we established that mTOR pathway hypoactivation is a converging molecular mechanism that contributes to two genetically distinct lissencephaly spectrum disorders, thus extending the continuum of mTORopathies, which until now have been characterized by pathway hyperactivity. Our findings suggest a clinically relevant molecular pathway for exploring potential treatments for lissencephaly spectrum disorders with distinct genetic causes. We speculate that the mTOR pathway may be a 'hidden hub' in disorders of cortical misfolding, with perturbation of different genes affecting mTOR signalling leading to distinct phenotypes (such as lissencephaly spectrum disorders or polymicrogyria). Thus, the mTOR pathway might represent a convergent point of intervention[49].

Online content

Any methods, additional references, Nature Portfolio reporting summaries, source data, extended data, supplementary information, acknowledgements, peer review information; details of author contributions and competing interests; and statements of data and code availability are available at https://doi.org/10.1038/s41586-024-08341-9.

1. Oegema, R. et al. International consensus recommendations on the diagnostic work-up for malformations of cortical development. *Nat. Rev. Neurol.* **16**, 618–635 (2020).
2. Di Donato, N. et al. Lissencephaly: expanded imaging and clinical classification. *Am. J. Med. Genet. A* **173**, 1473–1488 (2017).
3. Juric-Sekhar, G. & Hevner, R. F. Malformations of cerebral cortex development: molecules and mechanisms. *Annu. Rev. Pathol.* **14**, 293–318 (2019).
4. Severino, M. et al. Definitions and classification of malformations of cortical development: practical guidelines. *Brain* **143**, 2874–2894 (2020).
5. Barkovich, A. J., Dobyns, W. B. & Guerrini, R. Malformations of cortical development and epilepsy. *Cold Spring Harb. Perspect. Med.* **5**, a022392 (2015).
6. Wynshaw-Boris, A., Pramparo, T., Youn, Y. H. & Hirotsune, S. Lissencephaly: mechanistic insights from animal models and potential therapeutic strategies. *Semin. Cell Dev. Biol.* **21**, 823–830 (2010).
7. Bamba, Y. et al. In vitro characterization of neurite extension using induced pluripotent stem cells derived from lissencephaly patients with *TUBA1A* missense mutations. *Mol. Brain* **9**, 70–70 (2016).
8. Shahsavani, M. et al. An in vitro model of lissencephaly: expanding the role of DCX during neurogenesis. *Mol. Psychiatry* **23**, 1674–1684 (2018).
9. Koenig, M., Dobyns, W. B. & Di Donato, N. Lissencephaly: update on diagnostics and clinical management. *Eur. J. Paediatr. Neurol.* **35**, 147–152 (2021).
10. Iefremova, V. et al. An organoid-based model of cortical development identifies non-cell-autonomous defects in Wnt signaling contributing to Miller–Dieker syndrome. *Cell Rep.* **19**, 50–59 (2017).
11. Bershteyn, M. et al. Human iPSC-derived cerebral organoids model cellular features of lissencephaly and reveal prolonged mitosis of outer radial glia. *Cell Stem Cell* **20**, 435–449 (2017).
12. Lancaster, M. A. & Knoblich, J. A. Organogenesis in a dish: modeling development and disease using organoid technologies. *Science* **345**, 1247125 (2014).
13. Guzel, A. et al. Apparently novel genetic syndrome of pachygyria, mental retardation, seizure, and arachnoid cysts. *Am. J. Med. Genet. A* **143A**, 672–677 (2007).
14. Bilguvar, K. et al. The syndrome of pachygyria, mental retardation, and arachnoid cysts maps to 11p15. *Am. J. Med. Genet. A* **149A**, 2569–2572 (2009).
15. Sladky, V., Schuler, F., Fava, L. L. & Villunger, A. The resurrection of the PIDDosome—emerging roles in the DNA-damage response and centrosome surveillance. *J. Cell Sci.* **130**, 3779–3787 (2017).
16. Harripaul, R. et al. Mapping autosomal recessive intellectual disability: combined microarray and exome sequencing identifies 26 novel candidate genes in 192 consanguineous families. *Mol. Psychiatry* **23**, 973–984 (2018).
17. Sheikh, T. I. et al. Biallelic mutations in the death domain of PIDD1 impair caspase-2 activation and are associated with intellectual disability. *Transl. Psychiatry* **11**, 1 (2021).
18. Zaki, M. S. et al. Pathogenic variants in PIDD1 lead to an autosomal recessive neurodevelopmental disorder with pachygyria and psychiatric features. *Eur. J. Hum. Genet.* **29**, 1226–1234 (2021).
19. Di Donato, N. et al. Mutations in CRADD result in reduced caspase-2-mediated neuronal apoptosis and cause megalencephaly with a rare lissencephaly variant. *Am. J. Hum. Genet.* **99**, 1117–1129 (2016).
20. Harel, T. et al. Homozygous null variant in CRADD, encoding an adaptor protein that mediates apoptosis, is associated with lissencephaly. *Am. J. Med. Genet. A* **173**, 2539–2544 (2017).
21. Uctepe, E. et al. Bi-allelic truncating variants in CASP2 underlie a neurodevelopmental disorder with lissencephaly. *Eur. J. Hum. Genet.* **32**, 52–60 (2024).
22. Lancaster, M. A. et al. Cerebral organoids model human brain development and microcephaly. *Nature* **501**, 373–379 (2013).
23. La Manno, G. et al. Molecular architecture of the developing mouse brain. *Nature* **596**, 92–96 (2021).
24. Kang, H. J. et al. Spatio-temporal transcriptome of the human brain. *Nature* **478**, 483–489 (2011).
25. Weiler, E. S., Szabo, T. G., Garcia-Carpio, I. & Villunger, A. PIDD1 in cell cycle control, sterile inflammation and cell death. *Biochem. Soc. Trans.* **50**, 813–824 (2022).
26. Sladky, V. C. & Villunger, A. Uncovering the PIDDosome and caspase-2 as regulators of organogenesis and cellular differentiation. *Cell Death Differ.* **27**, 2037–2047 (2020).
27. Meng, D., Frank, A. R. & Jewell, J. L. mTOR signaling in stem and progenitor cells. *Development* **145**, dev152595 (2018).
28. Andrews, M. G., Subramanian, L. & Kriegstein, A. R. mTOR signaling regulates the morphology and migration of outer radial glia in developing human cortex. *eLife* **9**, e58737 (2020).
29. Takei, N. & Nawa, H. mTOR signaling and its roles in normal and abnormal brain development. *Front. Mol. Neurosci.* **7**, 28 (2014).
30. Saxton, R. A. & Sabatini, D. M. mTOR signaling in growth, metabolism, and disease. *Cell* **169**, 361–371 (2017).
31. Mao, B. et al. Overview of research into mTOR inhibitors. *Molecules* **27**, 5295 (2022).
32. Sengupta, S. et al. Discovery of NV-5138, the first selective brain mTORC1 activator. *Sci. Rep.* **9**, 4107 (2019).
33. Kato, T. et al. Sestrin modulator NV-5138 produces rapid antidepressant effects via direct mTORC1 activation. *J. Clin. Invest.* **129**, 2542–2554 (2019).
34. US National Library of Medicine. Phase 2 study of NV-5138 in adults with treatment resistant depression. *ClinicalTrials.gov* https://clinicaltrials.gov/ct2/show/results/NCT05066672 (2021).
35. LiCausi, F. & Hartman, N. Role of mTOR complexes in neurogenesis. *Int. J. Mol. Sci.* **19**, 1544 (2018).
36. Blair, J. D., Hockemeyer, D. & Bateup, H. S. Genetically engineered human cortical spheroid models of tuberous sclerosis. *Nat. Med.* **24**, 1568–1578 (2018).
37. D'Gama, A. M. et al. Mammalian target of rapamycin pathway mutations cause hemimegalencephaly and focal cortical dysplasia. *Ann. Neurol.* **77**, 720–725 (2015).
38. Mirzaa, G. M. et al. Association of *MTOR* mutations with developmental brain disorders, including megalencephaly, focal cortical dysplasia, and pigmentary mosaicism. *JAMA Neurol.* **73**, 836–845 (2016).
39. Salussolia, C. L., Klonowska, K., Kwiatkowski, D. J. & Sahin, M. Genetic etiologies, diagnosis, and treatment of tuberous sclerosis complex. *Annu. Rev. Genomics Hum. Genet.* **20**, 217–240 (2019).
40. Akula, S. K. et al. Exome sequencing and the identification of new genes and shared mechanisms in polymicrogyria. *JAMA Neurol.* **80**, 980–988 (2023).
41. Crino, P. B. mTOR signaling in epilepsy: insights from malformations of cortical development. *Cold Spring Harb. Perspect. Med.* **5**, a022442 (2015).
42. Li, Y. et al. Induction of expansion and folding in human cerebral organoids. *Cell Stem Cell* **20**, 385–396.e3 (2017).
43. Dang, L. T. et al. *STRADA*-mutant human cortical organoids model megalencephaly and exhibit delayed neuronal differentiation. *Dev. Neurobiol.* **81**, 696–709 (2021).
44. Blair, J. D., Hockemeyer, D., Doudna, J. A., Bateup, H. S. & Floor, S. N. Widespread translational remodeling during human neuronal differentiation. *Cell Rep.* **21**, 2005–2016 (2017).
45. Wang, L., Yao, J. & Hu, N. A mechanical method of cerebral cortical folding development based on thermal expansion. *Sci. Rep.* **9**, 1914 (2019).
46. Cunningham, C. L., Martínez-Cerdeño, V. & Noctor, S. C. Microglia regulate the number of neural precursor cells in the developing cerebral cortex. *J. Neurosci.* **33**, 4216–4233 (2013).
47. Warm, D., Schroer, J. & Sinning, A. GABAaergic interneurons in early brain development: conducting and orchestrated by cortical network activity. *Front. Mol. Neurosci.* **14**, 807969 (2021).
48. Bhaduri, A. et al. Cell stress in cortical organoids impairs molecular subtype specification. *Nature* **578**, 142–148 (2020).
49. Klingler, E., Francis, F., Jabaudon, D. & Cappello, S. Mapping the molecular and cellular complexity of cortical malformations. *Science* **371**, eaba4517 (2021).

Methods

Human participants

The study was approved by the Yale Human Investigation Committee (protocol number 9406007680). Institutional review board approvals for imaging studies, including written consent forms from all study participants, were obtained by the referring physicians at the participating institutions. There were no charges for participation.

WES analysis

WES was performed on three affected members of families NG8, NG375 and NG1801 following standard protocols. In brief, 1 µg genomic DNA obtained from peripheral blood samples was sheered using sonication. Library preparation was performed using a KAPA HyperPrep kit (Roche) and dual indices. Enrichment of the exome was performed using IDT xGen Exome Hyb Panel v.1 (NG8) and Nimblegen Roche v.2 human exome capture panel (NG375 and NG1801)16-plex multiplex capture. Purified and quantified libraries were sequenced on Illumina NovaSeq 6000 (NG8) and Hiseq 2500 (NG375 and NG1801) instruments using paired-end chemistry and 75 bp (NG375 and NG1801) and 100 bp (NG8) read lengths. Sufficient sequencing depth was obtained for all samples to call germline variants, as shown in Supplementary Table 3.

WES data analysis and variant identification

WES data analysis was performed using a pipeline developed in-house. This pipeline follows the GATK 4.1 best practices workflow for alignment and variant calling. In brief, raw FASTQ files were aligned to the human reference (GRCh38/hg38) using the Burrows–Wheeler Aligner tool (v.0.7.15). PCR duplicates were removed using MarkDuplicates (v.2.18.29) in Picard. The accuracy of each base call was estimated by applying BQSR. GATK 4.1.2 software was used to perform realignment of insertions and deletions and the generation of GVCF files using HaplotypeCaller. Once GVCF files were generated, joint variant calling was performed. Variant quality score recalibration was applied. Quality control was performed by checking the exome metrics summarizing the target-base coverage, genotypic sex (PLINK v.1.9), relationship inference (KING v.2.2.7) and contamination (Picard v.2.25.6). Variants were annotated using SnpEff (v.5.1), ANNOVAR and Ensembl Variant Effect Predictor (v.107) and an array of databases for variant allele frequency and effect on the encoded protein, conservation, tissue expression, deleteriousness and disease association. Variant filtration was performed according to variant sequencing quality (variant quality score recalibration of 'pass' and genotype quality score of ≥20), read depth (homozygous ≥ 4×, heterozygous ≥ 8×), minor allele frequency in gnomAD, 1K Genomes and an in-house, ethnically matched database of about 8,000 chromosomes (homozygous and compound heterozygous maximum allele frequency ≤ 0.005 and heterozygous ≤ 5×10^{-5}) and deleteriousness of missense variants (CADD v.1.6 Phred score ≥ 20). Only loss of function variants (canonical splice site, frameshift insertion or deletion and stop-gain) and deleterious missense variants were used for further analysis. A list of candidate variants is provided in Supplementary Table 1.

Isolation of hair follicle keratinocytes

About 8–10 hairs with intact follicles were removed from the scalp of patient NG375-1 using tweezers and placed in PBS (10010023; Thermo Fisher Scientific) containing antibiotic–antimycotic (15240062; Thermo Fisher Scientific) in a 60 mm dish. The shafts of the hairs were cut with sterile scissors so that only 2.5–5 cm remained attached to the follicle. Next, 0.25% trypsin–EDTA (25200056, Thermo Fisher Scientific) was added to the hair follicles for 10 min at 37 °C. Afterwards, a 1,000 µl pipette was used to pipette the trypsin solution on top of the follicle to ensure complete dissociation of the follicle from the hair, as confirmed under a microscope. The trypsin solution with follicle cells was inactivated by DMEM (11965092, Thermo Fisher Scientific) supplemented with 20% FBS (16141002, Thermo Fisher Scientific) in a 15 ml tube and centrifuged at 300*g* for 5 min. The follicular keratinocyte cells were resuspended in EpiLife+ human keratinocyte growth supplement (HKGS) (S0015, MEPI500CA, Thermo Fisher) containing 10 µM ROCK inhibitor (72304, Stem Cell Technologies). The cells were plated in 1 well of a 12-well plate coated with collagen matrix (R011K, Thermo Fisher Scientific) for 48 h at 37 °C. The medium was changed every day with EpiLife+ HKGS without ROCK inhibitor until keratinocytes could be seen. Keratinocytes were propagated using TrypLE select (12563011, Thermo Fisher Scientific) in tissue-culture-treated plates without collagen coating in subsequent passages.

Generation, characterization and maintenance of iPS cells

The MDLS iPS cell line was acquired from the Coriell Institute (GM26025). Agilent 60K Standard microarray comparative genomic hybridization was performed (Cell Line Genetics) on the MDLS cell line to confirm the chromosome 17p13.3 microdeletion. The R331X patient iPS cell line was generated using a CytoTune Sendai virus 2.0 kit (A16517, Thermo Fisher Scientific), in which hair follicle keratinocytes were transduced following the manufacturer's instructions for reprogramming fibroblasts using a feeder-dependent protocol. Two days before transduction, keratinocytes of passage 3 or lower were plated onto 1 well of a 6-well plate in EpiLife medium supplemented with HKGS and grown until 60% confluent. On day 0, CytoTune 2.0 Sendai virus was added to the cells and incubated overnight. The medium was replaced the next day (day 1) with fresh EpiLife medium plus HKGS, then daily until day 7. On day 6, culture dishes were prepared containing a feeder layer of irradiated CF1 mouse embryonic fibroblasts (MEFs; A34180, Thermo Fisher Scientific) culture dishes were prepared. On day 7, keratinocytes were trypsinized using TrypLE select for 5 min at 37 °C, diluted in DMEM/F12 (11320033, Thermo Fisher Scientific) and centrifuged at 300*g* for 5 min. The cells were resuspended in EpiLife medium plus HKGS and plated into 2 wells of a 6-well plate with CF1 MEFs. On day 8, the medium was changed to iPS cell medium consisting of DMEM/F12 20% knockout serum replacement (10828028, Thermo Fisher Scientific), 1× GlutaMax (35050061, Thermo Fisher Scientific), 1× MEM nonessential amino acids (11140050, Thermo Fisher Scientific), 100 µM β-mercaptoethanol (1985023, Thermo Fisher Scientific) and 10 ng ml^{-1} human FGF-2 (100-18B, Peprotech). From day 21 onwards, single iPS cell colonies were manually picked by scraping the colony and plating them in a fresh CF1 MEF feeder plate containing iPS cell medium. After expansion, the iPS cell colony was adapted to mTeSR Plus (Stem Cell Technologies, 100-0276) feeder-free conditions in the next passage. Outside-family control iPS cell lines were purchased from the Yale School of Medicine Stem Cell Core. All iPS cell lines were karyotyped and confirmed to be mycoplasma free (Cell Line Genetics). iPS cells were cultured in mTeSR Plus stem cell medium, and the medium was changed every day. iPS cells were passaged every 4–5 days using ReLeSR enzyme (100-0483, Stem Cell Technologies) onto new plates coated with Matrigel (354277, Corning). All studies were performed using approved safety protocols of the Yale School of Medicine.

CRISPR–Cas9 editing of iPS cells

Single-cell suspensions from iPS cell colonies were prepared using Accutase (07920, Stem Cell Technologies) and nucleofected using P3 Primary Cell nucleofector solution with supplement (V4XP-3032, Lonza), a donor single-stranded oligodeoxynucleotide (ssODN; IDT), a guide RNA (gRNA; IDT) and Cas9–GFP (76006, Stem Cell Technologies) using the Lonza 4D-Nucleofector system and Lonza program CA-137. Nucleofected single cells were transferred into mTESR Plus medium supplemented with CloneR supplement (05888, Stem Cell Technologies) and Alt-R HDR Enhancer (1081072, IDT). GFP-positive cells were collected 24 h after nucleofection by FACS and re-plated into a 96-well plate containing mTeSR Plus with CloneR supplement for clonal isolation at 1 cell per well. After the colony had grown to occupy

approximately 50% of the well surface area, one half of the colony was scraped using a pipette tip and collected into an Eppendorf tube for genomic DNA extraction using DirectPCR Lysis Reagent-Cell (301-C, Viagen) with proteinase K (501-PK, Viagen). Amplified PCR product containing the edit site was PCR-purified with a kit (28104, Qiagen) and sent for validation by Sanger sequencing. Sequence-verified CRISPR clones were subjected to karyotyping (Cell Line Genetics). The following primers, gRNAs and ssODNs were used: R331X mutation Sanger sequencing primers, GTCCATGCCTGCTGGAAG (forward) and AGGGG AGTCTGTCTGCCTGT (reverse); gRNAs, GGTCACTGAGCAGCCTCG AG (knock-in) and AGGGTCACTGAGCAGCC TCA (rescue); ssODNs, TGCAGGCGGACGCCACAGGCCAGGGTCACTGAGCAGCCTCAAGGGG TCACAGGAAAGCTGAGTGAGGAAGGAGCGAGCAAC (knock-in) and ACTGCAGGCGGACGCCACAGGCCAGGGTCACTGAGCAGCCTCGAGGG GTCACAGGAAAGCTGAGTGAGGAAGGAGCGAGCAAC (rescue).

Off-target analysis

Off-target analysis was performed using the Cas-OFFinder online program[50]. gRNA sequences for knock-in and rescue (as described above) were queried with a mismatch number of three or lower to generate a list of potential off-target sites, which were validated by Sanger sequencing. A total of 18 and 10 potential off-target sites were predicted with the gRNA used for editing patient into rescue iPS cells and control into knock-in iPS cells, respectively. Sanger sequencing of predicted off-target sites did not detect any mutations. Sequenced off-target sites are shown in Supplementary Fig. 2.

Generation of cerebral organoids

Unguided differentiation of organoids was performed using a STEMdiff Cerebral Organoid kit (08571, StemCell Technologies) for passage 20–40 of iPS cells. For each cell line, on D0, iPS cells were detached using Gentle Cell Dissociation reagent (100-0485, StemCell Technologies) for 8–10 min at 37 °C. Cells were resuspended in 1 ml embryoid body (EB) formation medium (basal medium 1 with supplement A). The suspension was centrifuged at 300*g* for 5 min and resuspended in 2 ml EB formation medium and 20 µM ROCK inhibitor. EB formation medium supplemented with 20 µM ROCK inhibitor was used to adjust the concentration to 100,000 cells per ml. Subsequently, 100 µl (10,000 cells per well) was added per well of a 96-well U-shaped-bottom low-attachment plate (174925, Thermo Fisher Scientific) and incubated for 48 h at 37 °C. On D2 and D4, 100 µl EB formation medium (without ROCK inhibitor) was added per well. On D5, 0.5 ml induction medium (basal medium 1 with supplement B) was added per well of a 24-well ultralow-attachment plate (3473, Corning) and 1–2 EBs were transferred into each well and incubated for 48 h at 37 °C. On D7, human embryonic stem cell-qualified Matrigel was thawed on ice for 1–2 h. Using a wide-bore 200-µl pipette tip, 25–50 µl of medium plus a single EB from 1 well of the 24-well plate was drawn up and transferred to 1 well of an organoid embedding sheet (08579, StemCell Technologies). Excess medium was removed. Using a pipette, 15 µl Matrigel was added onto each EB. The dish was subsequently placed in an incubator at 37 °C for 35 min to polymerize Matrigel. Using a 1-ml pipette tip, expansion medium (basal medium 2 with supplements C and D) was used to gently wash all Matrigel droplets off the embedding sheet into 1 well of an ultralow-attachment 6-well plate (3471, Corning) for a total of 3 ml expansion medium per well. Embedded organoids were incubated at 37 °C for 3 days. On day 10, the medium was replaced with 3 ml per well of maturation medium (basal medium 2 with supplement E or 08571, StemCell Technologies). The plate of organoids was placed on an Infors HT Celltron orbital shaker (I69222, Infors HT) at 70 rpm in a 37 °C incubator. A full change of maturation medium was performed every other day. On day 14, organoids were released from Matrigel droplets by incubating droplets on ice and in pre-cooled (2–8 °C) cell recovery solution (Corning, 354253) at 70 rpm on an orbital shaker. Afterwards, cell recovery solution was removed by washing in PBS 3 times, and maturation medium was added to organoids, for which the medium was changed in full every other day.

Treatment with the mTORC1 inhibitor NV-5138

NV-5138 (50 µM; HY-114384, MedChem Express) was added to the medium at D30 or D50 of organoid differentiation. Organoid medium containing the drug was changed every other day until D70, D100 or D120.

Organoid tissue preparation and immunohistochemistry

Whole organoids were fixed in 4% paraformaldehyde (PFA) in PBS (J61899, Thermo Fisher Scientific) at 4 °C overnight (about 16 h). Organoids were washed 3 times with PBS and then incubated in 30% sucrose solution overnight. Organoids were embedded in tissue freezing medium (72592, Electron Microscopy Sciences), sectioned with a cryostat (Leica) at 30–40 µm thickness and allowed to air dry overnight. For immunostaining, sections were washed 3 times for 10 min each with PBST (0.25% Triton-X in PBS) before adding blocking solution (0.25% Triton-X in PBS + 4% donkey serum (017-000-121, Jackson ImmunoResearch)) for 30 min at room temperature. Blocking solution was removed, and primary antibodies diluted in antibody solution (0.1% Triton-X in PBS + 4% donkey serum) were applied to the sections overnight (about 16 h) at 4 °C. After washing with PBST for 3 times (10 min each), secondary antibodies were applied for 1 h at room temperature (1:1,000), after which, sections were washed with PBS (3 times, 10 min each). To mark nuclei, DAPI (1:3,000; D1306, Thermo Fisher Scientific) was added to the secondary antibody incubation solution. Slides were then washed three times in PBS and mounted with VectaShield Vibrance Anti-Fade Mounting Medium (H-1700, Vector Labs). Images were acquired using a LSM 880 confocal microscope (Carl Zeiss) with identical settings across all conditions for each antibody, and images were collected using Zeiss Zen software and assembled using Fiji (National Institutes of Health).

Antibodies

The following primary antibodies were used: mouse anti-MAP2 (1:500; MAB3418, Millipore); mouse anti-SOX2 (1:500; sc-365823; Santa Cruz); rat anti-SOX2 (1:500; 14-9811-82, Invitrogen); rat anti-CTIP2 (1:500; ab18465; Abcam); rabbit anti-SATB2 (1:500; ab34735, Abcam); rabbit anti-TBR1 (1:500; ab31940, Abcam); rabbit anti-HOPX (1:2,500; HPA030180, Sigma); mouse anti-HOPX (1:250; sc-398703); rabbit anti-CC3 (1:1,000; 9661, Cell Signaling Technologies); mouse anti-PH3 (1:500; 9706, Cell Signaling Technologies); mouse anti-Ki67 (1:500; 556003, BD Biosciences); rabbit anti-EOMES (TBR2) (1:500; HPA028896, Sigma); sheep anti-EOMES (TBR2) (1:200; AF6166, R&D Systems); and rabbit anti-phospho-S6 ribosomal protein (pS6) (1:200; 4858, Cell Signaling Technologies). EdU assay was performed using a Click-It Plus Edu Cell Proliferation kit (C10337, Thermo Fisher Scientific) per the manufacturer's instructions.

PIDD1 protein structure

The predicted protein structure of PIDD1 was obtained from the AlphaFold Protein Structure Database[51,52].

Western blotting

Cold RIPA buffer (89900, Thermo Fisher Scientific) with protease and phosphatase inhibitors (5872, Cell Signaling Technologies) was used to lyse cerebral organoids or monolayer neural progenitor cells for 30 min on ice, followed by sonication using a Bioruptor Standard (Diagenode) at a high voltage setting for 5 cycles, 30 s on and 30 s off. Lysates were centrifuged at 14,000 rpm for 15 min and the supernatant was transferred into another Eppendorf tube. Protein concentration was measured using Bradford Coomassie Plus reagent (23238, Thermo Fisher Scientific) at an absorbance wavelength of 595 nm. Protein samples were equalized in concentration, and 4× Laemmli buffer

(1610747, Bio-Rad) with β-mercaptoethanol (1610710XTU, Bio-Rad) was added. The sample was boiled at 95 °C for 5 min and cooled on ice for 2 min. Lysates were loaded onto 12% TGX-mini protean gels (4561044, Bio-Rad), and electrophoresis was conducted at 100 V until the migration front reached the end of the gel cassette. Afterwards, the proteins were transferred to a PVDF membrane at 100 V for 1 h. After transfer, the PVDF membrane was allowed to dry overnight. PVDF was reactivated with methanol and blocked with EveryBlot blocking buffer (12010020, Bio-Rad) for 5 min. Then the following primary antibodies were added in EveryBlot buffer for 1 h at room temperature: mouse anti-PIDD1 (Anto-1) (1:500; ALX-804-837-C100, Enzo); rabbit anti-pS6 (1:1,000, 4858, Cell Signaling Technologies); rabbit anti-S6 ribosomal protein (5G10) (1:1,000; 2217, Cell Signaling Technologies); rabbit anti-phospho-AKT (S473) (1:1,000; 4060, Cell Signaling Technologies); rabbit anti-AKT (pan) (C67E7) (1:1,000; 4691, Cell Signaling Technologies); and mouse anti-β-actin (1:5,000; A2228, Sigma). The PVDF membrane was washed 4 times for 5 min each with TBST (Tris-buffered saline with 0.05% Tween-20). Then, anti-rabbit IgG, HRP (1:2,000; 7074, Cell Signaling Technologies) and anti-mouse IgG, HRP (1:2,000–5,000; 7076, Cell Signaling Technologies) were added in EveryBlot Buffer for 1 h at room temperature. The membrane was washed 4 times for 5 min each in TBST, and Clarity Western ECL substrate (1705061, Bio-Rad) was added for 5 min at room temperature to detect proteins using film-based imaging. All wash and antibody-incubation steps were performed under agitation. For stripping of antibodies, the PVDF membrane was incubated in Restore Plus Stripping buffer (46430; Thermo Fisher Scientific) for 15 min at room temperature with agitation on a shaker, followed by TBST washes (3 times, 10 min each), EveryBlot blocking and incubation with a different antibody. Uncropped and unprocessed images of western blots are provided in Supplementary Fig. 1.

scRNA-seq

Sample preparation. Organoids were collected and single-cell suspensions were prepared using a Neural Tissue Dissociation kit (130-092-628; Miltenyi Biotec). Single-cell suspensions were loaded onto a Chromium Controller (10x Genomics) for droplet formation. scRNA-seq libraries were prepared using a Chromium Single Cell 3′ Reagent kit (10x Genomics). Samples were sequenced on NovaSeq 6000 instruments.

Quality control analysis. After receiving raw sequencing files, the human GRCh38 (GENCODEv32/Ensembl98) genome (https://www.ncbi.nlm.nih.gov/datasets/genome/GCF_000001405.26) /was used as the reference genome to run the CellRanger (v.6.1.2) pipeline, including read alignment, barcode counting and unique molecular identifier (UMI) quantification. This resulted in the filtered raw count matrices containing gene expression in all inferred cells for downstream quality control. R (v.4.3.0)[53] and Seurat (v.4.3.0)[54] were used for data processing. An initial clustering for each individual of each species was conducted, and low-quality clusters with low UMIs (<500) and high mitochondrial content (>10%) were removed. Genes expressed in at least three cells were kept for downstream analysis. The remaining cells were re-clustered, and doublet scores were calculated using the DoubletFinder package. Gene expression in each cell was then normalized using the NormalizeData function in the R package Seurat[54] (scaling factor = 10,000).

Transcriptomic integration of the scRNA-seq data of organoids from different genotypes. To embed all cells from different organoids in the same low-dimensional space and to subsequently visualize them on the UMAP, the data were integrated using Seurat. Specifically, for each individual sample, the top 5,000 highly variable genes were identified using the variance-stabilizing transformation (FindVariableFeatures function) implemented in Seurat, and the top 2,000 highly variable genes were selected for integration using the SelectIntegrationFeatures function. Anchors were identified across datasets using the function FindIntegrationAnchors based on the top 50 dimensions from canonical correlation analysis, followed by hierarchical integration of normalized data using the IntegrateData function. Genes expressed in fewer than 100 cells were filtered out, the integrated data were scaled, principal components analysis was performed and significant principal components were selected using elbow plots. These principal components were used for downstream UMAP visualization.

Clustering and annotation. Well-established organoid markers were used to annotate all the cell types[55–57]. Samples were clustered into the following cell classes: immature excitatory neuron (DCX, STMN2 and GAP43); upper layer excitatory neuron (NEUROD2, SATB2 and FRMD4B); deep layer excitatory neuron (BCL11B, TBR1 and NEUROD2); RG (SOX2); oRG (SOX2, HOPX, FAM107A and LIFR); dividing progenitor (SOX2, MKI67 and TOP2A); intermediate progenitor (EOMES and TMEM158); proliferating intermediate progenitor (EOMES, TMEM158, MKI67 and TOP2A); and astrocyte (S100B and GFAP). DEGs and GO analyses in different conditions (control, patient, knock-in and rescue) for each cell type were identified using the default setting for the function (FindAllMarkers) in Seurat. An average $\log_2$-transformed fold change of >0.3 and an adjusted P value of <0.05 were used as thresholds to find significant DEGs using the two-tailed Wilcoxon rank-sum test. The cor() function in R with method = 'pearson' was used to calculate the gene expression correlation (r). The R package TopGO was used for GO analysis with all protein-coding genes as the background gene list.

MS analysis

Protein and sample preparation. Organoids were suspended in 400 µl RIPA buffer containing protease and phosphatase inhibitor cocktail (3×). Two bursts (10% amp) of sonication for 15 s each with on–off for 1 s were carried out to lyse the tissue samples. The cell suspension was centrifuged at 14,000 rpm for 10 min, and 125 µl of the supernatant was removed. Chloroform–methanol–water protein precipitation was performed, and dried protein pellets were each resuspended in 75 µl 8 M urea containing 400 mM ABC, reduced with DTT alkylated with iodoacetamide, and enzymatic digestion with trypsin was performed for 3 h and followed with additional trypsin (0.1 µl of 0.5 µg µl^{-1}) for overnight digestion at 37 °C. The digestion solution (total volume of 200 µl) was quenched (with 10.1 µl of 20% trifluoroacetic acid) during the desalting step with C18 MacroSpin columns (The Nest Group). The effluents from the desalting step were dried and re-dissolved in 50 µl buffer solution (LB, 98% H_2O, 2% acetonitrile and 0.2% trifluoroacetic acid). An aliquot was taken, the concentration measured using a Nanodrop instrument and the sample diluted to 0.06 µg µl^{-1} with LB. A 1:4 dilution of 10× Pierce Retention Time Calibration mixture (88321) was added to each sample before injecting into a UPLC Q-Exactive HFX mass spectrometer to check the retention time.

Label-free quantification

Data collection. Label-free quantification data-dependent acquisition was performed using a Thermo Scientific Q-Exactive HFX mass spectrometer connected to a Waters M-Class Acquity ultra-performance liquid chromatography (UPLC) system equipped with a Waters Symmetry C18 180 µm × 20 mm trap column and a 1.7 µm, 75 µm × 250 mm nanoAcquity UPLC column (35 °C). Next, 5 µl of each digest was reconstituted in loading buffer A to a concentration of 0.05 µg µl^{-1} and injected in a block-randomized order. UPLC peptide trapping was carried out for 3 min at 5 µl min^{-1} in 99% buffer A (0.1% formic acid in water) and 1% buffer B (0.075% formic acid in acetonitrile) before eluting with linear gradients that reached 6% B at 2 min, 25% B at 200 min and 85% B at 205 min. Three blanks (first with 100% acetonitrile, second and third with buffer A) followed each injection to ensure against sample carryover. The following settings for the Q-Exactive HFX mass spectrometer were used: 120,000 MS scan resolution with an automatic gain control (AGC) target of 3×10^6 (max IT of 100 ms) and scan range

of 350–1,500 *m/z* in profile mode; 30,000 MS2 scan resolution with an AGC target of 1×10^5 (max IT of 100 ms) and scan range of 200–2,000; and top 20 peptide higher-energy collisional dissociation (HCD) fragmentation consisting of an isolation window of 1.6 *m/z*, normalized collision energy of 28, peptide match preferred with all multiple charge states, and dynamic exclusion of 20.0 s. All MS and MS/MS peaks were detected in the Orbitrap.

Data analysis. The LC–MS/MS data were processed using Progenesis QI software (Nonlinear Dynamics, v.4.2) with protein identification carried out using an in-house Mascot search engine (2.8). The Progenesis QI software performs chromatographic and spectral alignment (one run is chosen as a reference for alignment of all other data files), mass spectral peak picking and filtering (the ion signal must be at least 3 times the s.d. of the noise) and quantification of proteins and peptides. A normalization factor for each run was calculated to account for differences in sample load between injections and differences in ionization. The normalization factor was determined by calculating a quantitative abundance ratio between the reference run and the run being normalized, with the assumption being that most proteins or peptides are not changing in the experiment so that the quantitative value should be equal to 1. The experimental design was set up to group multiple injections (technical and biological replicates) from each run into each comparison set. The algorithm then calculated the tabulated raw and normalized abundances and ANOVA *P* values for each feature in the dataset. The MS/MS spectra were exported as.mgf (Mascot generic files) for database searching. The Mascot search algorithm was used for searching against the Swiss Protein database with taxonomy restricted to *Homo sapiens*, and carbamidomethyl (Cys), oxidation (Met), phospho (Ser, Thr and Tyr), deamidation (NQ) and acetylation (K, protein N termini) were entered as variable modifications. Two missed tryptic cleavages were allowed, precursor mass tolerance was set to 10 ppm and fragment mass tolerance was set to 0.02 Da. The significance threshold was set based on a false discovery rate (FDR) of 2% with 95% MOWSE score confidence levels. The Mascot search results were exported as .xml files and then imported into the processed dataset in Progenesis QI software, in which identified peptides were synced with the corresponding quantified features and their corresponding abundances. Protein abundances (requiring at least one unique peptide with scores above the significant threshold) were then calculated from the sum of all unique normalized non-conflicting peptide ions for a specific protein on each run. Resulting label-free quantification data were exported, and comparative analyses were calculated in Excel. To detect significant differences in protein abundances between conditions, we performed a *t*-test using the package of Bioconductor (v.3.18)[58], with a FDR threshold of 0.1. Significantly upregulated or downregulated proteins were functionally annotated using the Reactome 2022 pathway and MSigDB 2020 Hallway databases. Pathways with FDR *q* values < 0.05 were considered significant.

Riboprobe synthesis

RNA probes complementary to human *PIDD1* were synthesized from cDNA templates of *PIDD1* 5′ (forward primer: 5′-CAGGAGATGCT TCAGAGGATTC-3′; reverse primer: 5′-GTCCAAATCTGAGGTCAGG AAC-3′; size 926 bp) and *PIDD1* 3′ (forward primer: 5′-TCTGGTACAC CACCAAGAACTG-3′; reverse primer: 5′-GGATGCTGTCCTGGTAC TTGC-3′; size 879 bp) sequences through in vitro transcription and labelled with digoxigenin-11-UTP (11277073910, Roche).

In situ hybridization

Human fetal brain tissue and cerebral organoids were fixed by immersion in 4% PFA (in PBS), cryoprotected in 30% sucrose (in 4% PFA) and sectioned on a cryomicrotome (Leica Microsystems). Sections (30–40 µm) were mounted on SuperFrost slides (12-550-143, Thermo Fisher Scientific), dried overnight and processed for in situ hybridization. In brief, the sections were post-fixed in 4% PFA (15 min), washed in PBS (3 times, 5 min each), treated with proteinase K (10 µg ml^{-1}, 30 min; 3115879001, Roche), post-fixed in 4% PFA (15 min), rinsed in PBS and transferred to a hybridization solution (50 µg ml^{-1} heparin (H4784, Sigma), 200 µg ml^{-1} acetylated BSA (00630517, Invitrogen), 500 µg ml^{-1} brewer's yeast tRNA (10109525001, Roche), 50% formamide (295876, Sigma) and 5× SSC, 1% SDS) containing 0.1–0.5 µg ml^{-1} digoxigenin-labelled riboprobe. Hybridization was allowed to proceed overnight at 70 °C. Three 45-min washes were performed with solution X (1% SDS, 2× SSC and 50% formamide) at 70 °C, followed by washes with TBST (3 times, 15 min each). Sections were incubated in 10% heat-inactivated lamb serum (16070096, Thermo Fisher Scientific) for 1 h at room temperature, and then in TBST containing 1% lamb serum and 1:5,000 dilution of alkaline phosphatase-coupled anti-digoxigenin, Fab fragments (11093274910, Roche) for 2 h at room temperature. Post-antibody washes consisted of 3 TBST changes (15 min each). Histochemical detection of alkaline phosphatase activity was performed using the chromogen combination of nitro blue tetrazolium (350 mg ml^{-1}; 11383213001, Roche) and 5-bromo-4-chloro-indoxyl phosphatase (175 mg ml^{-1}; 11383221001, Roche) in alkaline phosphatase reaction buffer NTMT (100 mM Tris-HCl pH 9.5, 100 mM NaCl, 50 mM $MgCl_2$ and 1% Tween-20). After completion of the colour reaction, sections were washed in TBST, dehydrated and mounted with Eukitt (15322, Electron Microscopy Sciences). Sections were analysed using a Stemi stereomicroscope or an AxioImager (Zeiss) fitted with an AxioCam MRc5 digital camera. Images were captured using AxioVision software (Zeiss) and assembled in Adobe Photoshop.

Golgi–Cox staining of organoids

D120 organoids were fixed in 4% PFA and processed using a FD Rapid GolgiStain kit (PK401, FD Neurotechnologies). Organoids were sectioned at 70 µm, mounted on gelatinized slides and processed for Golgi staining following the manufacturer's instructions.

Functional effect of the nonsense single-nucleotide variant in *PIDD1*

The single-nucleotide variant identified in the patient from the NG375 family is predicted to introduce a premature stop codon and to result in truncation of the PIDD1 protein, possibly triggering nonsense-mediated decay. *PIDD1* transcript levels were compared in control, patient and rescue organoids at D70 with and without treatment with 50 µM cycloheximide for 2 h. Organoids were then analysed by RT–qPCR for the *PIDD1* transcript (forward primer: 5′-GAGCAGCCACCCTTTGCG; reverse primer: 5′-CTCGCATCTGCAGGACACA), with *GAPDH* as an internal control (forward primer: 5′-TGGTCTCCTCTGACTTCAACAGCG; reverse primer: 5′-AGGGGTCTACATGGCAACTGTGAG).

Immunostaining and western blot quantifications

All quantifications were performed using Fiji. Only cortical structures or regions on the periphery of the organoid were analysed. Cortical structures with visible apical and basal sides, appropriate morphology (distinct progenitor and neuronal layers, see below) and healthy appearance were chosen for quantification.

We defined organoid layers based on a previous study using the same organoid generation protocol[56]. Ventricular length was defined as an uninterrupted stretch of apical surface populated by RG, as shown by PH3 or RG marker (SOX2 or PAX6) staining. The VZ was defined as a layer of cells directly abutting the ventricle, with a distinctive radial organization of nuclei and high density of cells, as revealed by DAPI staining, and may be positive for SOX2 or PAX6. The SVZ was defined as a zone basally adjacent to the VZ but apically adjacent to the CP that contains cells expressing HOPX or TBR2. The progenitor zone was defined as the combined area of the VZ and the SVZ. The CP was defined as the area staining positive for neuronal markers such as CTIP2, SATB2 and TBR1.

The total thickness of the CP, the SVZ and the VZ was determined by a 90° vertical line extending from the ventricular apical surface to the basal surface. The relative thickness of each layer was calculated by normalizing the thickness of each layer (defined as described above) to the combined thickness of the VZ, the SVZ and the CP.

All cell counts were normalized per mm^2 area unless indicated otherwise. All organoid immunostaining quantifications were performed using at least two independent organoid batches. When quantifying co-localization, the cell was double positive only if the signal from both channels analysed clearly corresponded in shape.

Western blot quantifications were performed using the Analyze-Gels functions of ImageJ, and proteins of interest were normalized to the β-actin loading control.

Quantification and statistics

Quantifications are represented as scatter plots (with the centre black line representing the mean) or as bar graphs (with error bars representing the s.d.). Statistical analysis was performed using GraphPad Prism 10.3.1 software. Tests for significance on image quantification values were performed using ordinary one-way ANOVA or ordinary two-way ANOVA, with an α level of 0.05 and Tukey's test (one-way) and Dunnett's test (two-way) to correct for multiple comparisons, or two-tailed unpaired *t*-test with an α level of 0.05. *P* values are indicated in figures by asterisks. *P* values for all quantifications are listed in Supplementary Table 5.

Reporting summary

Further information on research design is available in the Nature Portfolio Reporting Summary linked to this article.

Data availability

Summary statistics for WES data analyses are provided in Supplementary Tables 1 and 3. Individual-level phenotype data of patients with *PIDD* mutations are provided in Supplementary Table 2. Sequencing data of patients with *PIDD1* mutations are publicly restricted owing to consent forms not allowing broad sharing of raw genomic data. scRNA-seq files have been deposited into the Sequence Read Archive with accession number PRJNA1168541. MS data have been deposited into the Proteomics Identification Database with accession number PXD056364. Deposited files associated with figures for scRNA-seq and MS are provided in Supplementary Table 6. AlphaFold (https://alphafold.ebi.ac.uk) was used to predict the PIDD1 protein structure. Human Brain Transcriptome (https://hbatlas.org/pages/hbtd) was used to display *PIDD1* mRNA expression across brain regions and developmental time points. Pathway enrichment analysis was performed using the MSigDB 2020 Hallmark gene set from GSEA (https://www.gsea-msigdb.org/gsea/index.jsp), the OMIM disease dataset (https://www.omim.org) and the Reactome 2022 pathway database (https://reactome.org/).

Code availability

Our scRNA-seq and MS R pipelines have been deposited into GitHub (github.com/danliangunc/PIDD1-lissencephaly) with no restrictions.

50. Bae, S., Park, J. & Kim, J.-S. Cas-OFFinder: a fast and versatile algorithm that searches for potential off-target sites of Cas9 RNA-guided endonucleases. *Bioinformatics* **30**, 1473–1475 (2014).
51. Jumper, J. et al. Highly accurate protein structure prediction with AlphaFold. *Nature* **596**, 583–589 (2021).
52. Varadi, M. et al. AlphaFold Protein Structure Database in 2024: providing structure coverage for over 214 million protein sequences. *Nucleic Acids Res.* **52**, D368–D375 (2024).
53. The R Development Core Team. *R: A Language and Environment for Statistical Computing* (R Foundation for Statistical Computing, 2024).
54. Hao, Y. et al. Integrated analysis of multimodal single-cell data. *Cell* **184**, 3573–3587 (2021).
55. Velasco, S. et al. Individual brain organoids reproducibly form cell diversity of the human cerebral cortex. *Nature* **570**, 523–527 (2019).
56. Kelava, I., Chiaradia, I., Pellegrini, L., Kalinka, A. T. & Lancaster, M. A. Androgens increase excitatory neurogenic potential in human brain organoids. *Nature* **602**, 112–116 (2022).
57. Xiang, Y. et al. HESC-derived thalamic organoids form reciprocal projections when fused with cortical organoids. *Cell Stem Cell* **24**, 487–497 (2019).
58. Ritchie, M. E. et al. limma powers differential expression analyses for RNA-sequencing and microarray studies. *Nucleic Acids Res.* **43**, e47 (2015).

Acknowledgements We are indebted to the patients and families who contributed to this study. We thank A. Dincer, M. Estancion, R. Fulbright, J. Guo, M. Olivero-Acosta and Y. Yang for experimental advice; C. Castaldi, M. Shibata and I. Tikhonova for assistance with experiments; F. Collin and W. Wang for proteomic sample preparation and data collection; and D. McGuone and A. Poulopoulos for discussions. The schematic in Extended Data Fig. 3a was created using BioRender (https://www.biorender.com). This work was supported by the Departments of Neurosurgery and Genetics (Yale School of Medicine), Acibadem University and National Institutes of Health (NIH) grants R01HD110693 (to A.L. and K.B.), T32GM007205 (Medical Scientist Training Program training grant), RC2NS070477 (to M.G.), R01MH103616 (to M.G. and K.B.), UM1HG006504 (to M.G and S.M.) and MH124619, MH116488, MH122678, MH130991 and DA053628 (to N.S.). The Yale Center for Genome Analysis, the Keck Microarray Shared Resource and the MS and Proteomics Resource at Yale University are funded by Yale University and Yale School of Medicine and by the Office of the Director of the NIH (S10OD030363, S10OD02365101, S10OD019967 and S10OD018034).

Author contributions C.Z., A.L. and K.B. conceived the study and wrote the manuscript. C.Z. designed the experiments, generated and validated all iPS cell lines and cerebral organoids, and performed and analysed all iPS cell and organoid experiments. D.L. performed bioinformatic analyses. A.G.E.-S. supervised experimental work. A.S.B., J.C., I.Q.C., O.H., S.N., X.W., A.B.P., Y.T., C.C., A.N. and K.M.-G. supported experimental work. A.N. assisted with gRNA design. F.L.-G. assisted with whole-genome sequencing. T.T.L. assisted with MS analyses. M.N.K., T.B., K.Y. and E.Z.E.-O. assisted with analyses and maintenance of the Yale Neurogenetics cohort. D.F.M. contributed to bioinformatic analyses. C.Y. interpreted patient MRI scans. G.W. assisted with scRNA-seq. S.M. provided WES support. H.K., A.G., A.O.C. and B.T. recruited patients. N.S. supervised bioinformatic analyses. M.G. established the Yale Neurogenetics cohort, and conceptualized and led gene discovery in this cohort. A.L. designed, performed and analysed experiments, and supervised experimental work. K.B. designed and supervised the genetic and transcriptomic experiments and analyses. A.L. and K.B. led the research.

Competing interests N.S. is a co-founder and shareholder of Bexorg, Inc. All the other authors declare no competing interests.

Additional information

Supplementary information The online version contains supplementary material available at https://doi.org/10.1038/s41586-024-08341-9.

Correspondence and requests for materials should be addressed to Murat Gunel, Angeliki Louvi or Kaya Bilguvar.

Peer review information *Nature* thanks Stephanie Baulac and the other, anonymous, reviewer(s) for their contribution to the peer review of this work. Peer reviewer reports are available.

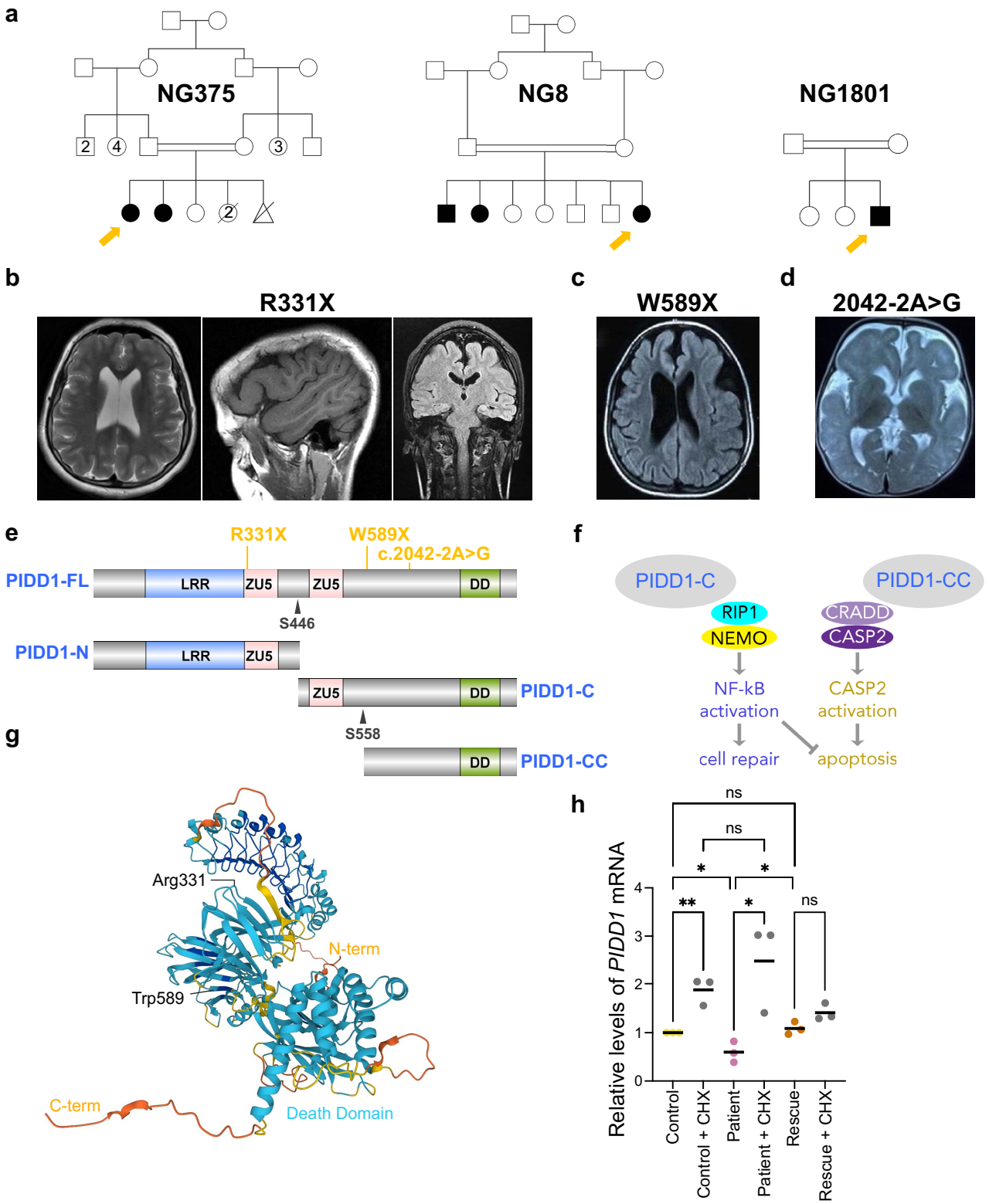

Extended Data Fig. 1 | See next page for caption.

Extended Data Fig. 1 | Homozygous mutations in *PIDD1* are associated with lissencephaly spectrum disorders. a, Simplified pedigrees for the NG375, the NG8, and the NG1801 families with the indicated mutations in *PIDD1*. **b**, Magnetic resonance images (MRI) of the index case and iPS cell donor NG375-1 (arrow); axial (T2-weighted), sagittal and coronal (T1-weighted) images demonstrating bilateral diffuse pachygyria; the upper and middle gyri in the temporal lobes are diffusely and symmetrically thickened and smooth; no microgyria was observed; the ventricles are large. **c**,**d**, Axial images of index cases (arrows) from the NG8 (**c**, T1-weighted) and NG1801 families (**d**, T2-weighted) demonstrating diffuse pachygyria. **e**, Domain structure of the PIDD1 full-length (FL) protein indicating serine autoproteolysis sites (arrowheads) and resulting fragments PIDD1-N, PIDD1-C, and PIDD1-CC. The locations of the stop-gain (R331X, W589X) and canonical splice-site (c.2042-2A>G) mutations (vertical lines) are indicated on PIDD1-FL. **f**, PIDD1-FL derived C-terminal fragments PIDD1-C and PIDD1-CC containing the death domain participate in complexes with either RIP1-NEMO ("NEMO-PIDDosome") or CRADD-Caspase-2 (CASP2) ("CASP2-PIDDosome") to regulate cell survival or apoptosis, respectively. **g**, Protein structure of PIDD1 (UniProt ID: Q9HB75) generated by AlphaFold with indicated N- and C-termini (yellow), death domain (light blue), and stop-gain mutation sites (black). **h**, Quantification of relative expression levels of *PIDD1* mRNA from RT-qPCR of organoids at D70 treated with 50 μM cycloheximide (CHX) for 2 h and untreated counterparts. $n = 3$ organoids, 3 independent experiments per genotype. Statistical test: Two-tailed unpaired t test: **, $P < 0.01$*, $P < 0.05$, ns, not significant. LRR: leucine-rich repeats; ZU5: domain present in ZO-1 and Unc5-like netrin receptors; DD: death domain.

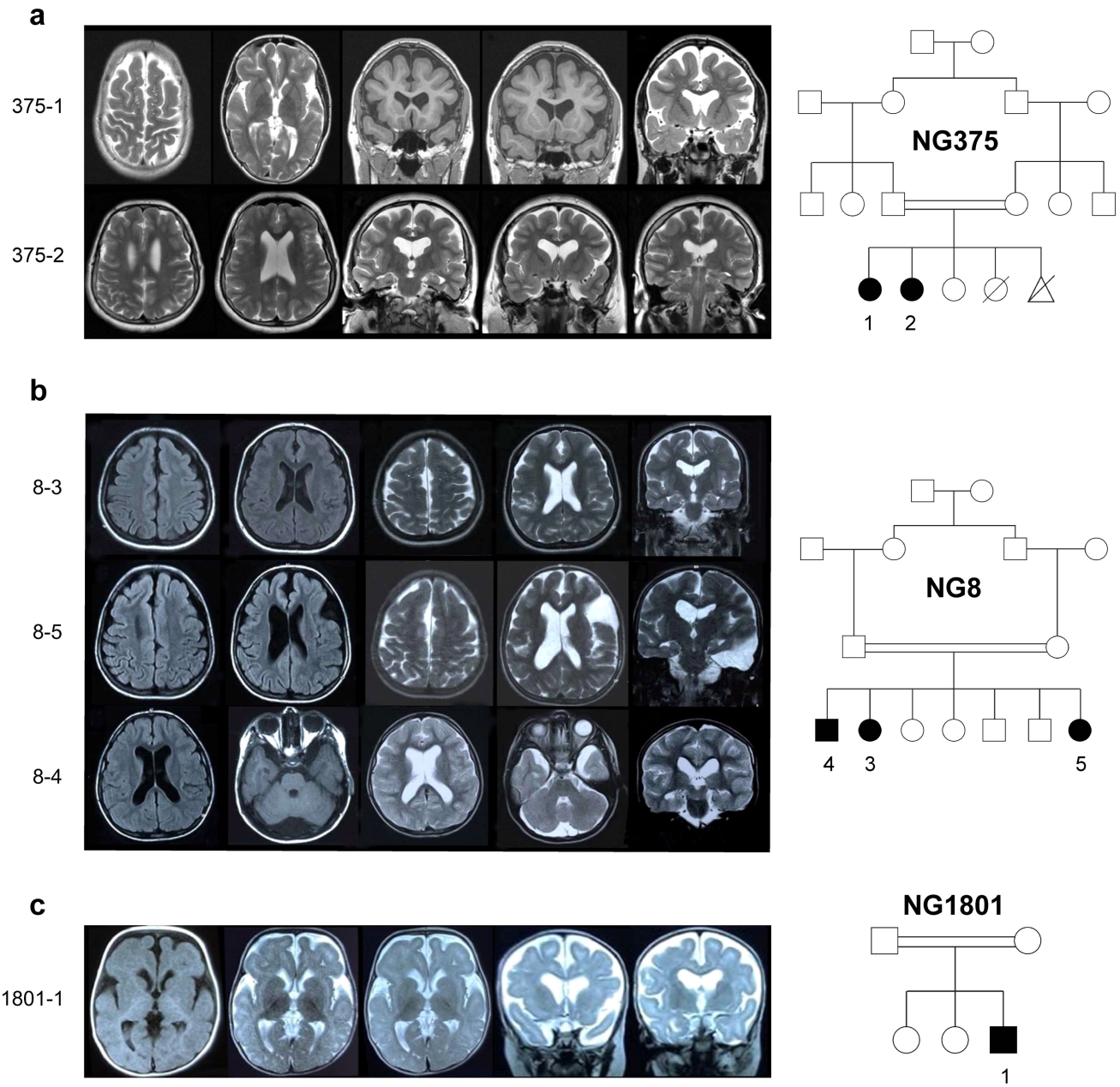

Extended Data Fig. 2 | Magnetic Resonance Imaging (MRI) of affected individuals with mutations in *PIDD1*. **a**, NG375 family. Axial T2-weighted and coronal T1- and T2-weighted MR images of two siblings with the stop-gain R331X mutation, showing cortical thickening, simplification of gyri, and fronto-temporal atrophy. **b**, NG8 family. Axial T1- and T2-weighted and coronal T2-weighted MR images of three siblings with the stop-gain W589X mutation. Axial T1-weighted and T2-weighted MR images with bilateral and diffuse thickening of the cortex and simplification of gyri with an anterior > posterior gradient. Coronal T2-weighted MR images with diffuse pachygyria. Enlargement of the subarachnoid spaces consistent with arachnoid cysts are also noted. **c**, NG1801 family. Axial T1- and T2-weighted and coronal T2-weighted MR images of one individual with the c.2042-2A>G splice-site mutation, showing frontal pachygyria and simplification of gyri.

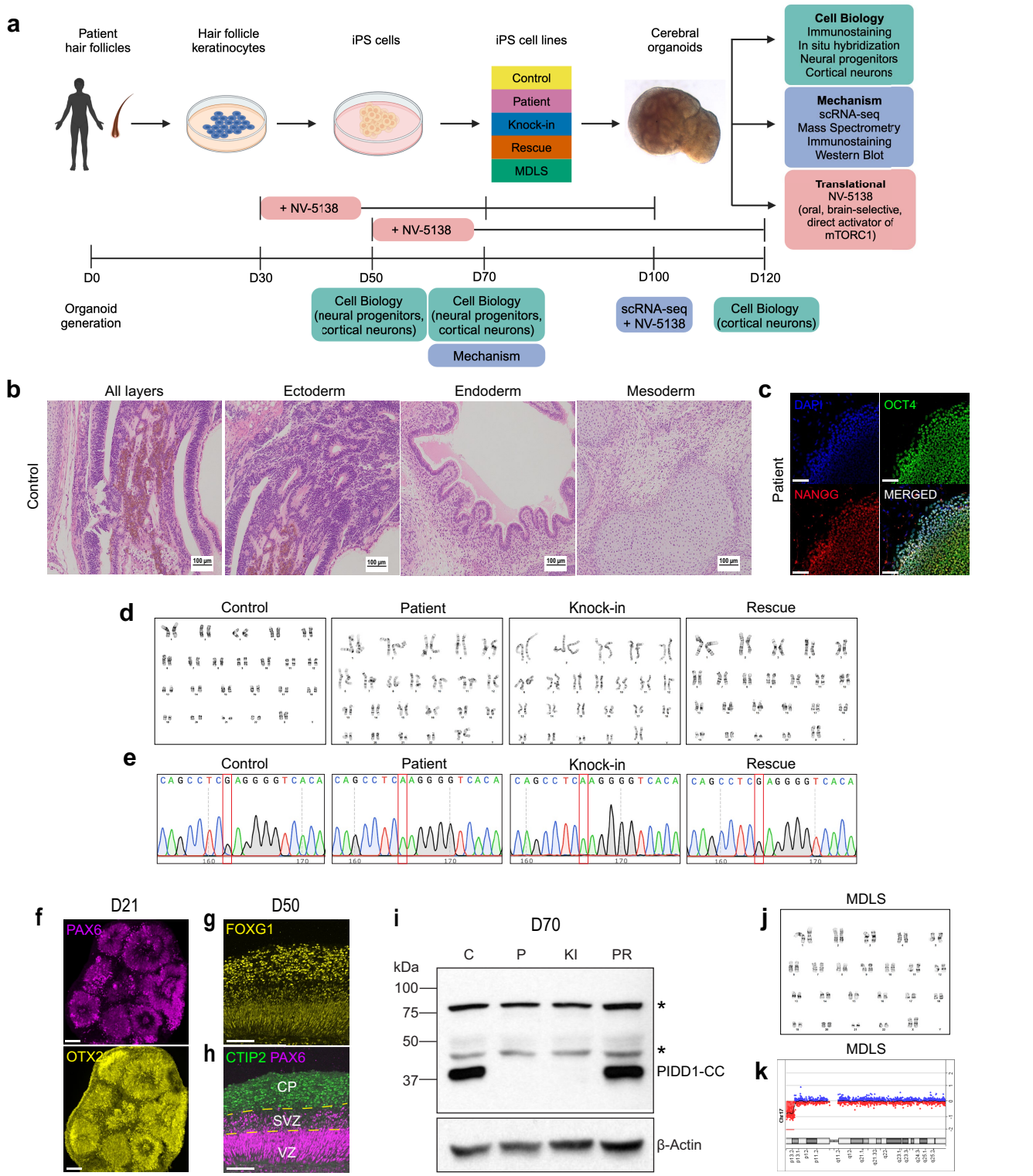

Extended Data Fig. 3 | Study design and generation and characterization of iPS cells and cerebral organoids. a, Schematic of the workflow. **b**, Sample images of cell types of three germ layers in teratomas from control iPS cells following transplantation to SCID mice, $n = 1$ experiment. **c**, Immunostaining of patient iPS cells for pluripotency markers OCT4 and NANOG, $n = 1$ iPS cell colony. **d**, Karyotypes for control, patient, knock-in, and rescue iPS cells. **e**, Sanger sequencing chromatograms for control, patient, knock-in, and rescue iPS cells. Red boxes indicate wild-type or mutated sites. **f**, Immunostaining for dorsal neural progenitor markers PAX6 and OTX2 in an organoid at D21, $n = 1$ organoid. **g**,**h**, Immunostaining for dorsal forebrain markers FOXG1 (**g**) and CTIP2 and PAX6 (**h**) in an organoid at D50, $n = 1$ organoid. **i**, Western blot of organoid lysates at D70, with antibodies against a C-terminal PIDD1 epitope and beta-actin (loading control); PIDD1-CC (~37 kDa), $n = 2$ experiments (mixture of 3 organoids) per genotype. Asterisks indicate non-specific bands. For gel source data, refer to Supplemental Fig. 1b. **j**, Karyotype for MDLS iPS cells. **k**, Chromosome 17 array comparative genomic (aCG) hybridization output profile for the MDLS iPS cells. CP: cortical plate, SVZ: subventricular zone, VZ: ventricular zone. Scale bars, 100 µm. The schematic in **a** was created using BioRender (credit: C.Z., https://biorender.com/w12b840; 2023). Scale bars, 100 µm.

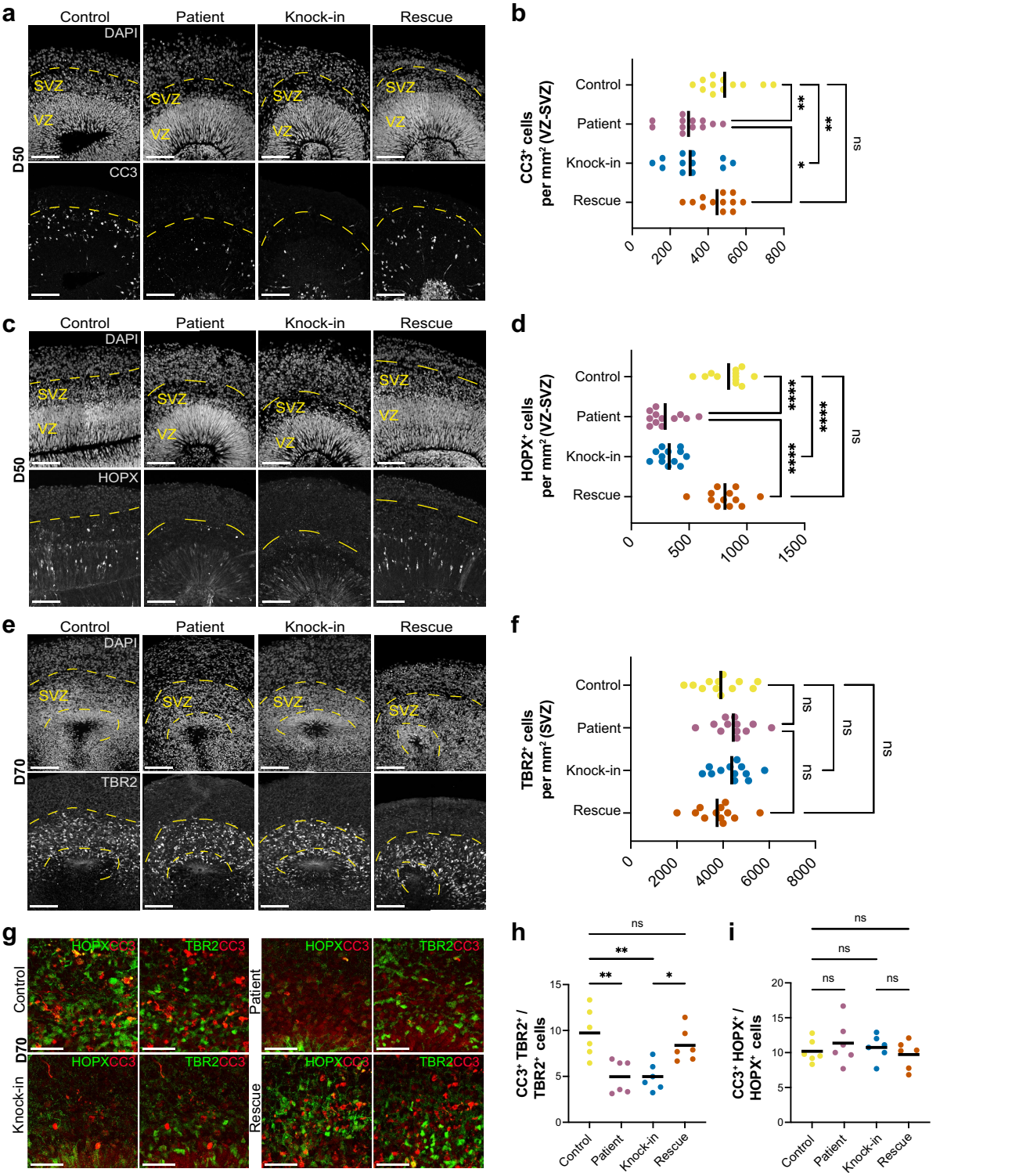

Extended Data Fig. 4 | Neural progenitor cell abnormalities in PIDD1-mutant organoids. a, Control, patient, knock-in, and rescue organoids at D50 immunostained for apoptotic cell marker cleaved-caspase 3 (CC3). Dashed yellow lines delineate the SVZ/VZ. **b**, Quantification of $CC3^+$ cells per mm^2 SVZ/VZ area. **c**, Control, patient, knock-in, and rescue organoids at D50 immunostained for oRG cell marker HOPX. Dashed yellow lines delineate the SVZ/VZ. **d**, Quantification of $HOPX^+$ cells per mm^2 SVZ/VZ area. **e**, Control, patient, knock-in, and rescue organoids at D70 immunostained for IPC marker TBR2. Dashed yellow lines delineate the SVZ. **f**, Quantification of $TBR2^+$ cells per mm^2 SVZ area. **g**, Control, patient, knock-in, and rescue organoids at D70 immunostained for oRG marker HOPX, TBR2, and CC3. **h**, **i**, Quantification of the faction of $CC3^+$ cells co-expressing either TBR2 (**h**) or HOPX (**i**). $n = 12$ cortical regions, $n = 6$ organoids, 2 batches of 3 organoids per genotype (**b, d, f**); $n = 6$ cortical regions, $n = 6$ organoids, 2 batches per genotype (**h, I**). Statistical test: one-way ANOVA; ****, $P < 0.0001$; **, $P < 0.01$; *, $P < 0.05$; ns, not significant. Scale bars, 100 µm (**a, c, e**) and 50 µm (**g**).

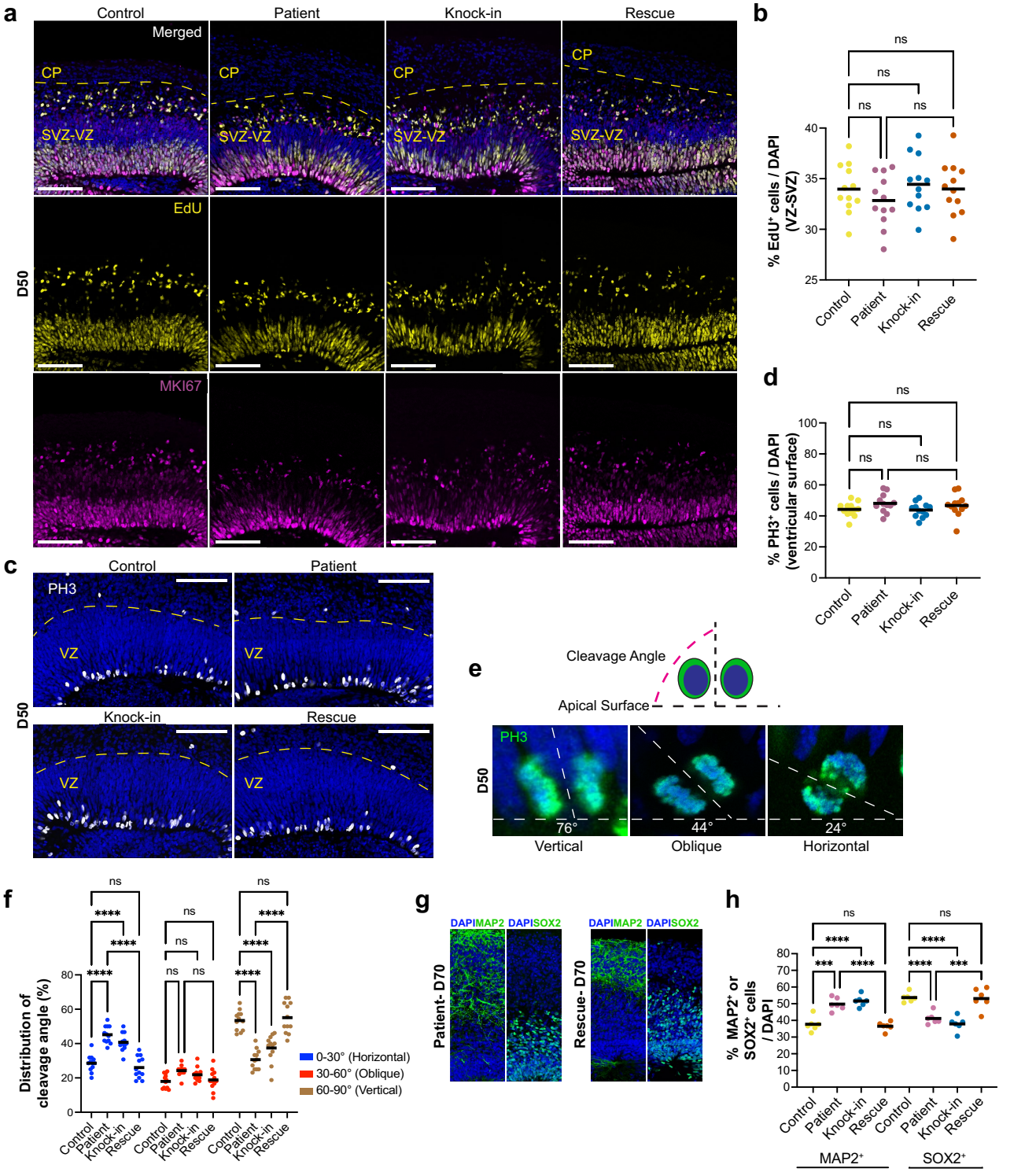

Extended Data Fig. 5 | Increased neurogenesis in PIDD1-mutant organoids. **a**, Control, patient, knock-in, rescue organoids at D50 immunostained for EdU and MKI67 (also known as Ki67). Dashed yellow lines delineate the CP and SVZ/VZ. **b**, Quantification of EdU$^+$ cells in SVZ/VZ. **c**, Immunostaining for phospho-histone H3 (PH3) in the VZ. **d**, Quantification of PH3$^+$ cells at the ventricular surface. **e**, Diagram illustrating cleavage angle measurement (top); representative examples of vertical, oblique, and horizontal divisions in PH3$^+$ cells (bottom). Nuclei are stained with DAPI. **f**, Quantification of the cleavage angle (relative to apical surface) in PH3$^+$ cells. **g**, Immunostaining for differentiating neuron marker MAP2 and SOX2 in cortical region of patient and rescue organoids at D70. **h**, Quantification of MAP2$^+$ and SOX2$^+$ cells in a cortical region of control, patient, knock-in, and rescue organoids at D70. $n = 12$ cortical regions, $n = 6$ organoids, 2 batches of 3 organoids per genotype (**b, d**); dividing apical progenitor cells from $n = 12$ organoids were counted per genotype (**f**); $n = 6$ cortical regions, $n = 6$ organoids, 2 batches per genotype (**h**). For (**g**), $n = 6$ cortical regions, $n = 3$ organoids per genotype. Statistical test: one-way ANOVA per genotype; ****, $P < 0.0001$; ***, $P < 0.001$; ns, not significant. Scale bars, 100 µm.

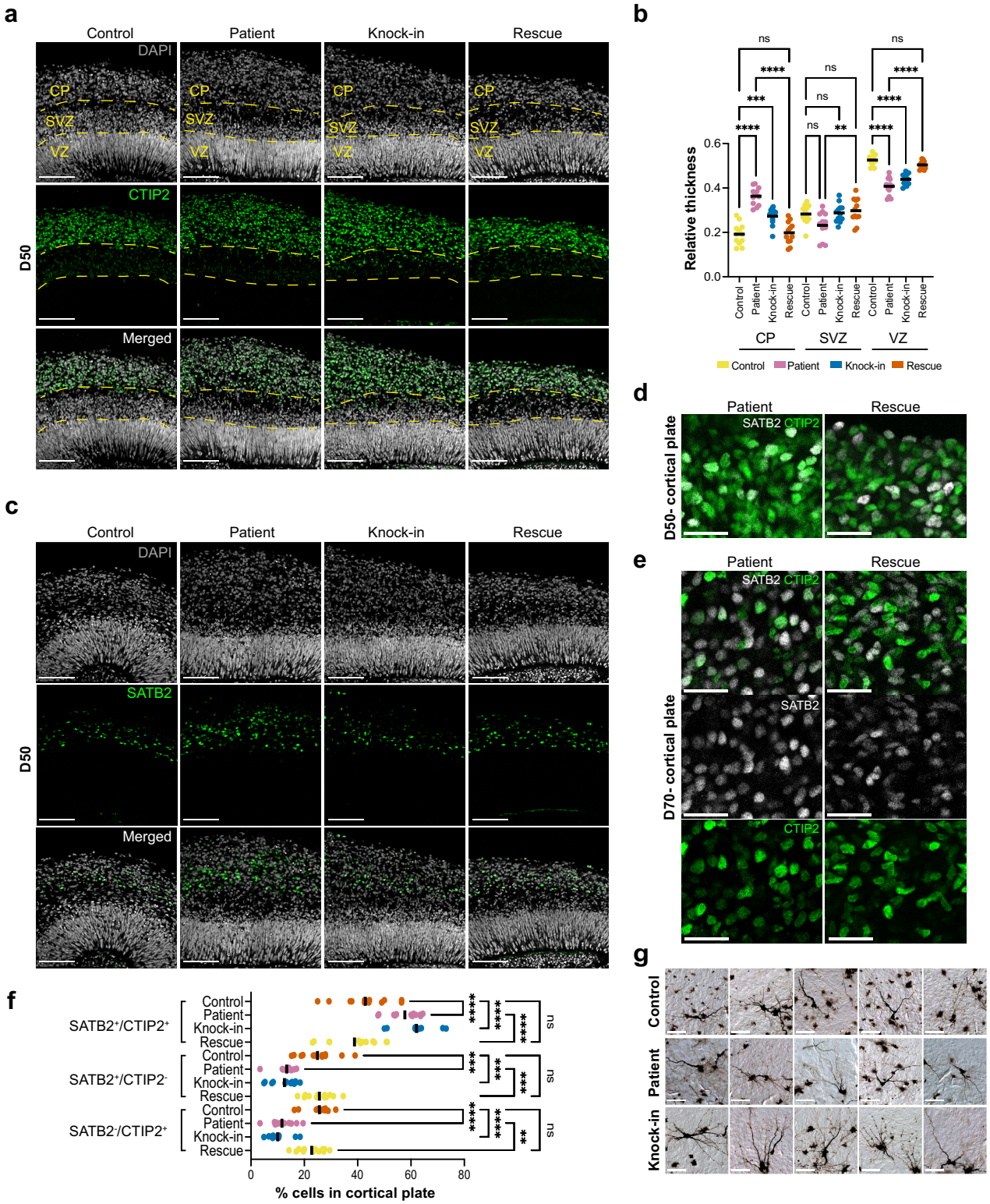

Extended Data Fig. 6 | Cortical plate defects in PIDD1-mutant organoids. **a**, Control, patient, knock-in, and rescue organoids at D50 immunostained for deep-layer neuron marker CTIP2. Dashed yellow lines delineate the CP, SVZ, and VZ. **b**, Quantification of relative thickness of VZ, SVZ, and CP. **c**, Control, patient, knock-in, and rescue organoids at D50 immunostained for upper-layer neuron marker SATB2. **d**-**e**, Patient and rescue organoids at D50 (**d**) and at D70 (**e**) immunostained for CTIP2 and SATB2. **f**, Quantification of $SATB2^{+}/CTIP^{+}$, $SATB2^{+}/CTIP2^{-}$ and $SATB2^{-}/CTIP2^{+}$ cells in CP. **g**, Golgi-Cox staining of neurons in the upper CP of control, patient, and knock-in organoids at D120. Pial surface is to the top. All experiments were performed with images from $n = 12$ cortical regions, $n = 6$ organoids, 2 batches of 3 organoids per genotype. Statistical test: one-way ANOVA; ****, $P < 0.0001$; ***, $P < 0.001$; **, $P < 0.01$; ns, not significant. Scale bars, 100 µm (**a, c, d**) and 50 µm (**e, g**).

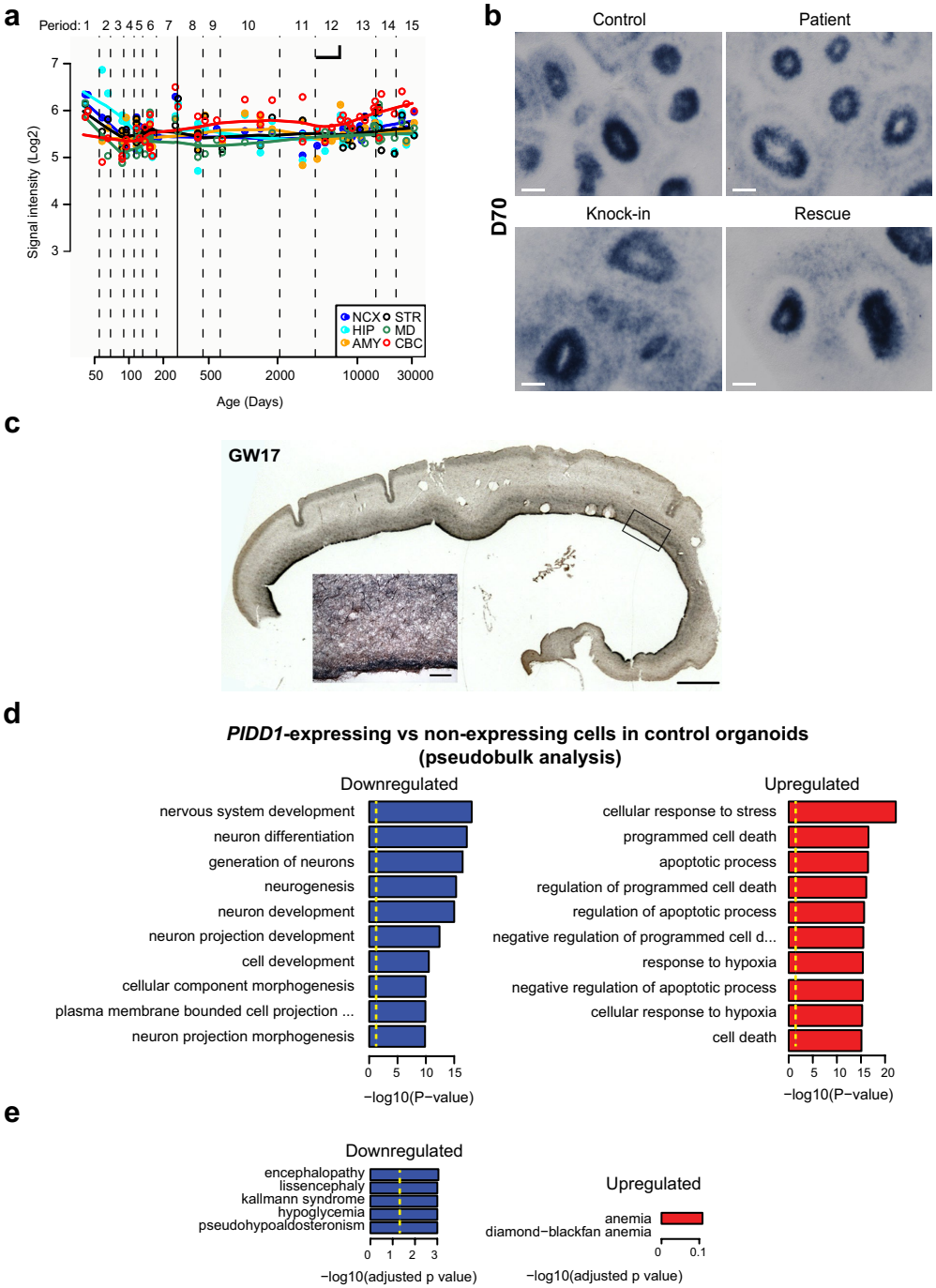

Extended Data Fig. 7 | Analyses of *PIDD1* mRNA expression. a, *PIDD1* exon array signal intensity in human fetal, postnatal, and adult brain (hbatlas.org). **b,c**, Representative images of sections of control, patient, knock-in, and rescue organoids at D70, ($n = 4$ organoids per genotype) (**b**) and sections of human fetal cortex at gestational week (GW) 17 (**c**) following in situ hybridization with a probe detecting the 3′ end of the *PIDD1* transcript. Inset (**c**) shows a high-magnification view of the area delineated by a black rectangle. **d**, GO enrichment analysis for biological processes of *PIDD1*-expressing vs non-expressing cells in control organoids at D70. Bar graphs of downregulated (left) and upregulated (right) GO pathways for *PIDD1*-expressing compared with non-expressing cells in control organoids (pseudobulk analysis). **e**, Disease enrichment analysis of *PIDD1*-expressing cells in control vs patient organoids using the OMIM expanded dataset. Bar graphs of downregulated (left) and upregulated (right) GO pathways. GO analysis was performed using all *PIDD1*-expressing and non-expressing cells in patient ($n = 4$) vs control ($n = 4$) organoids. Two-tailed Fisher's exact test and $P < 0.05$ was used as the threshold for analyses in (**d, e**). Scale bars, 2 mm (**b, c**), 50 µm (**c,** inset). NCX: neocortex; HIP: hippocampus; AMY: amygdala; STR: striatum; MD: mediodorsal nucleus of the thalamus; CBC: cerebellar cortex.

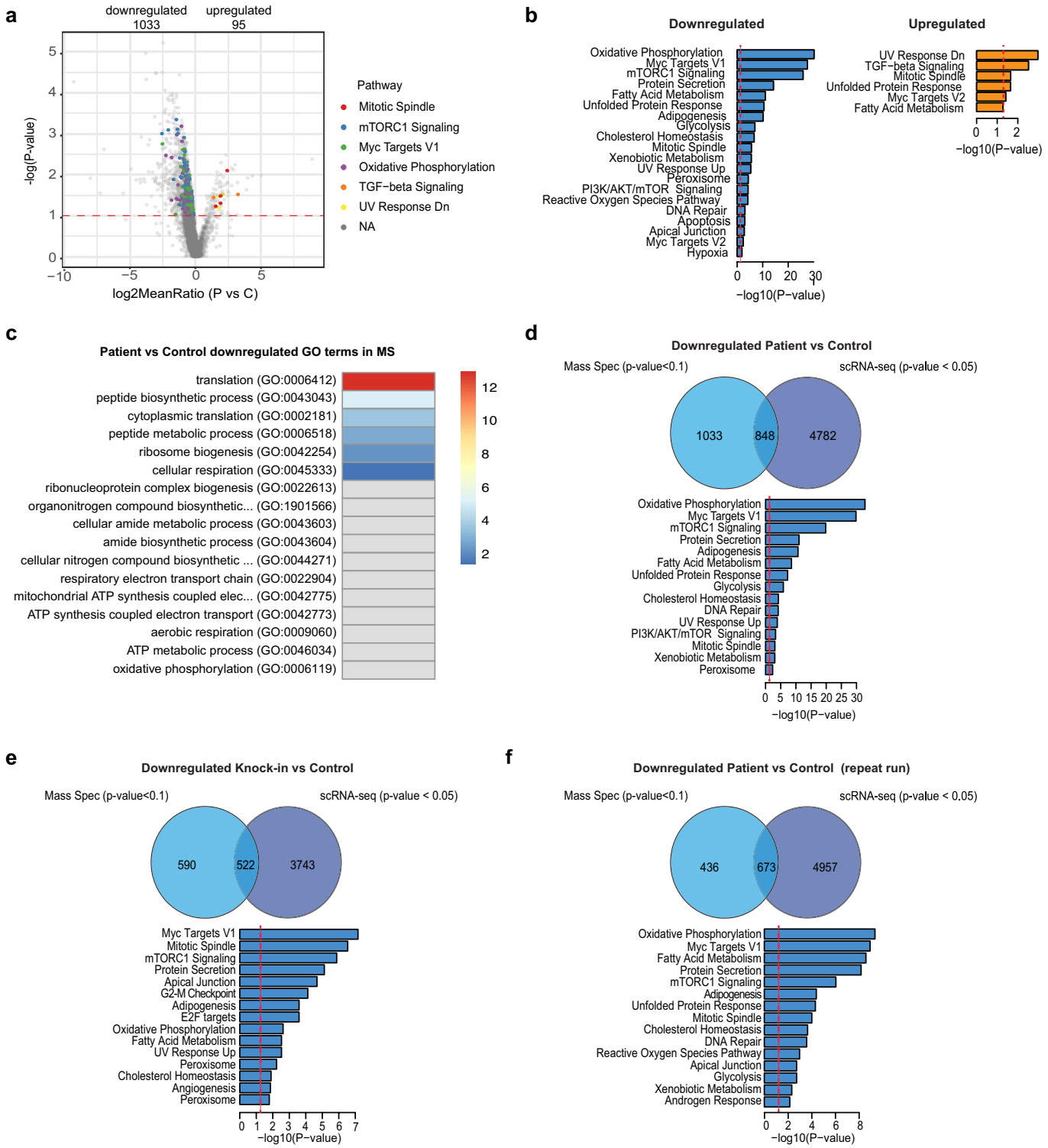

Extended Data Fig. 8 | Comparison of transcriptomic and proteomic datasets of PIDD1-mutant organoids. a-b, Volcano plot of DEPs and selected pathways (**a**) and PE analysis (**b**) for patient vs control organoids at D70 analyzed by MS; bar graphs of downregulated (left) and upregulated (right) pathways in patient organoids. **c**, Heatmap of downregulated GO terms shared between patient and control scRNA-seq (RG cluster) and MS datasets. Colour bar represents -log(adjusted *P* value). Grey boxes indicate GO terms that were not significantly downregulated for the comparison. **d-f**, Venn diagrams and pathway analysis of shared downregulated DEGs/DEPs in scRNA-seq (oRG cell-type) and MS datasets from patient vs control (**d**), knock-in vs control (**e**), and patient vs control (repeat analyses) (**f**). The MSigDB2020 Hallmark gene set from GSEA was used in all pathway analyses. In (**a**) a *P* value of 0.1 was used as threshold for determining DEPs. PE analysis was conducted with a *P* value threshold of 0.05 using two-tailed Fisher's exact test. Control, $n = 3$; patient, $n = 3$ batches, 3 organoids per batch, were analyzed per MS experiment. The patient vs control dataset in this figure and the knock-in vs control dataset in Fig. 4 are from two independent MS experiments.

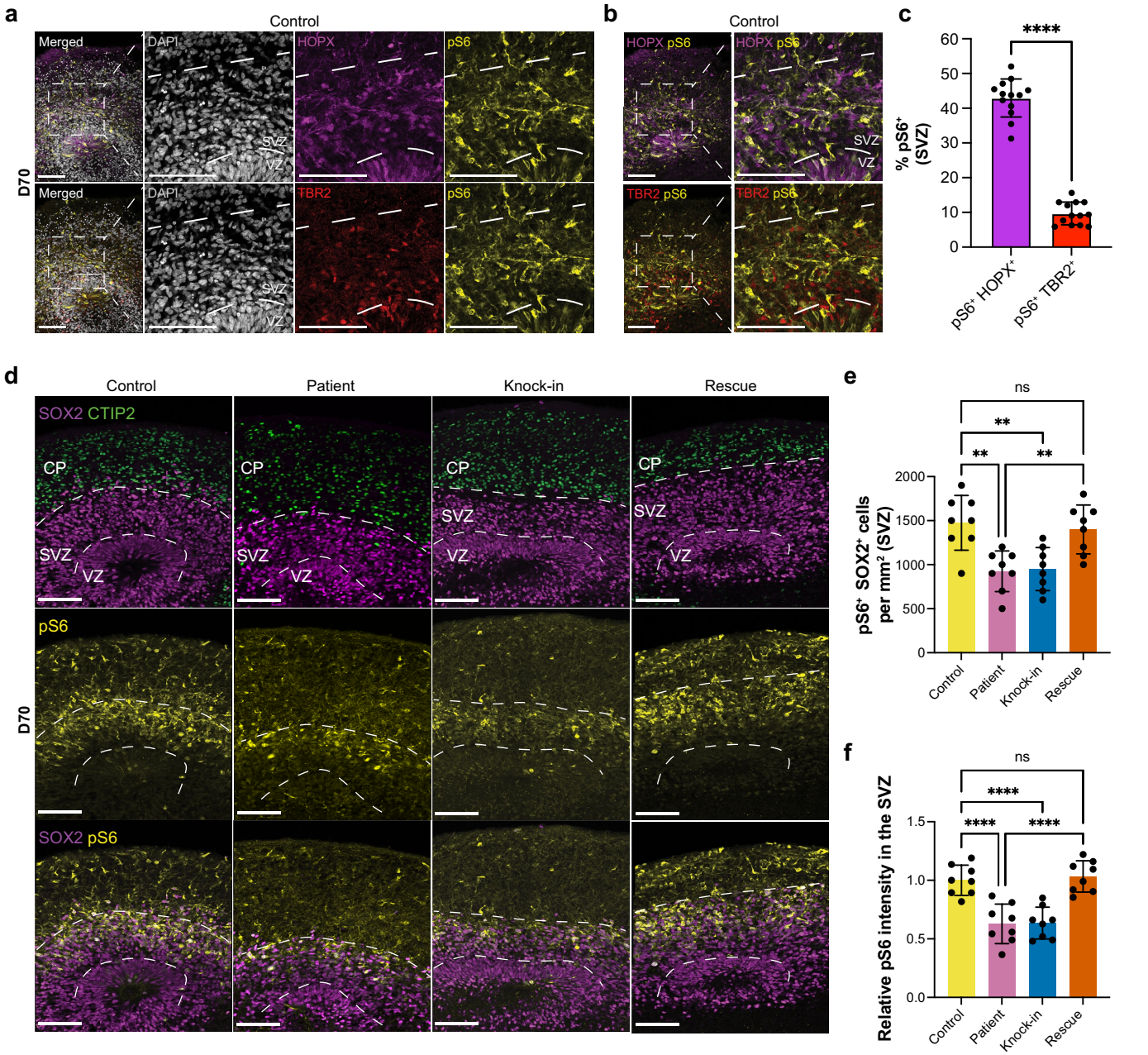

Extended Data Fig. 9 | Hypoactive mTOR signalling in SVZ progenitors of PIDD1-mutant organoids. a-b Control organoids at D70 immunostained for pS6 and oRG marker HOPX or IPC marker TBR2. Nuclei are stained with DAPI. Dashed white box indicates the magnified area shown to the right; dashed white lines delineate the SVZ/VZ. **c**, Quantification of $HOPX^+/pS6^+$ or $TBR2^+/pS6^+$ cells in the SVZ. **d**, Control, patient, knock-in, and rescue organoids at D70 immunostained for SOX2, CTIP2, and pS6. **e**, Quantification of $pS6^+/SOX2^+$ cells per mm^2 SVZ area. **f**, Quantification of pS6 relative intensity in the SVZ area. $n = 13$ cortical regions, $n = 6$ organoids, 2 batches of 3 organoids per genotype (**c**); $n = 8$ cortical regions, $n = 4$ organoids, 2 batches of 2 organoids per genotype (**e, f**). Statistical tests: two-tailed unpaired t-test; ****, $P < 0.0001$ (**c**); one-way ANOVA; ****, $P < 0.0001$; **, $P < 0.01$; ns, not significant (**e, f**). Data are mean±s.d. (**c, e, f**). Scale bars, 100 µm.

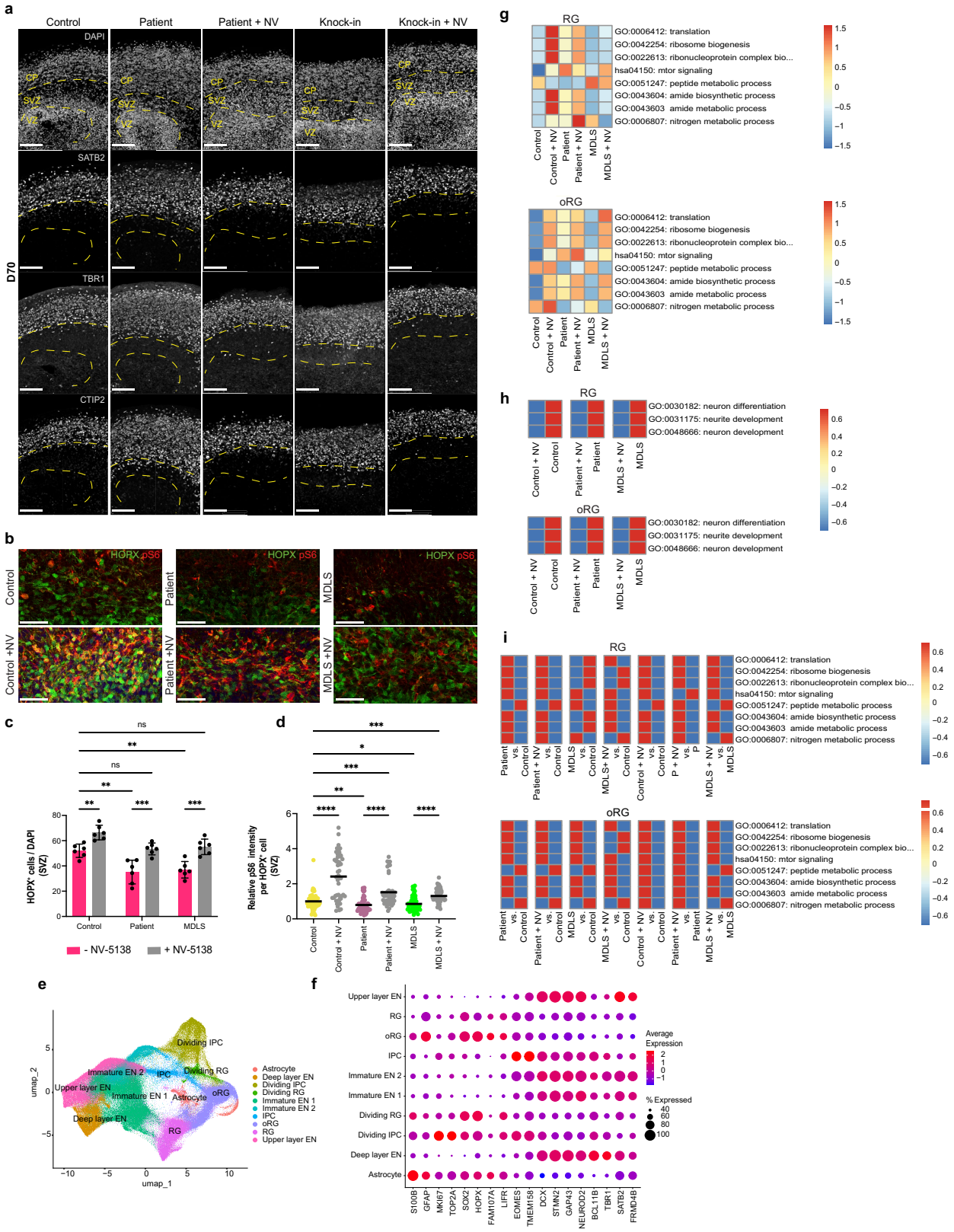

Extended Data Fig. 10 | See next page for caption.

Extended Data Fig. 10 | An mTORC1 activator rescues cellular defects and upregulates mTOR signalling, translation, and metabolism in PIDD1-mutant organoids. a, Control, patient, and knock-in organoids at D70 grown with or without NV-5138 (NV) immunostained for CP markers CTIP2, TBR1, and SATB2. Dashed yellow lines delineate the CP, SVZ, and VZ. **b**, Control, patient, and MDLS organoids at D70 grown with or without NV-5138 (NV) immunostained for oRG cell marker HOPX and pS6. **c**, Quantification of HOPX-expressing cells in the SVZ. **d**, Quantification of pS6 relative intensity in HOPX-expressing cells in the SVZ. **e**, UMAP projection of all cells from scRNA-seq of control, patient, and MDLS organoids at D70. EN, excitatory neuron. **f**, Dot plot expression of selected established marker genes used for cell-type classification of entire dataset. **g**, Normalized average pseudo-bulk gene expression in RG cells (upper) and oRG cells (bottom) for gene sets related to selected GO terms in different conditions. Colour bar represents -log10 (adjusted *P* value). **h**, Paired comparison for normalized average pseudo-bulk gene expression in RG cells (upper) and oRG cells (bottom) for gene sets related to selected neuron-related GO terms in different conditions. Colour bar represents scaled gene expression. **i**, Paired comparison for normalized average pseudo-bulk gene expression in RG cells (upper) and oRG cells (bottom) for gene sets related to selected translation and metabolism-related GO terms in different conditions. Colour bars represent scaled gene expression. $n = 6$ cortical regions, $n = 6$ organoids, two batches per genotype (**c**); $n = 50$ cells, $n = 4$ organoids, two batches of two organoids per genotype (**d**). Statistical tests: two-tailed unpaired t-test (**c**); ***, $P < 0.001$; **, $P < 0.01$; ns, not significant; one-way ANOVA (**d**); ****, $P < 0.0001$; ***, $P < 0.001$; **, $P < 0.01$; *, $P < 0.05$. Organoids analyzed by sc-RNAseq: control, $n = 2$; control + NV, $n = 2$; patient, $n = 2$, patient + NV, $n = 2$, MDLS, $n = 2$, MDLS + NV, $n = 2$. Data are mean±s.d. (**c**). Scale bars, 100 µm (**a**) and 50 µm (**b**).

nature portfolio

Corresponding author(s): Angeliki Louvi, Murat Gunel, Kaya Bilguvar

Last updated by author(s): 3 October 2024

Reporting Summary

Nature Portfolio wishes to improve the reproducibility of the work that we publish. This form provides structure for consistency and transparency in reporting. For further information on Nature Portfolio policies, see our Editorial Policies and the Editorial Policy Checklist.

Statistics

For all statistical analyses, confirm that the following items are present in the figure legend, table legend, main text, or Methods section.

n/a	Confirmed
☐	☒ The exact sample size (*n*) for each experimental group/condition, given as a discrete number and unit of measurement
☐	☒ A statement on whether measurements were taken from distinct samples or whether the same sample was measured repeatedly
☐	☒ The statistical test(s) used AND whether they are one- or two-sided *Only common tests should be described solely by name; describe more complex techniques in the Methods section.*
☒	☐ A description of all covariates tested
☐	☒ A description of any assumptions or corrections, such as tests of normality and adjustment for multiple comparisons
☐	☒ A full description of the statistical parameters including central tendency (e.g. means) or other basic estimates (e.g. regression coefficient) AND variation (e.g. standard deviation) or associated estimates of uncertainty (e.g. confidence intervals)
☐	☒ For null hypothesis testing, the test statistic (e.g. *F*, *t*, *r*) with confidence intervals, effect sizes, degrees of freedom and *P* value noted *Give P values as exact values whenever suitable.*
☒	☐ For Bayesian analysis, information on the choice of priors and Markov chain Monte Carlo settings
☒	☐ For hierarchical and complex designs, identification of the appropriate level for tests and full reporting of outcomes
☐	☒ Estimates of effect sizes (e.g. Cohen's *d*, Pearson's *r*), indicating how they were calculated

Our web collection on statistics for biologists contains articles on many of the points above.

Software and code

Policy information about availability of computer code

Data collection	NovaSeq 6000 (Illumina) and HiSeq 2500 (Illumina), Zeiss Zen
Data analysis	Single-cell RNA seq and mass spec R pipeline is deposited at github.com/danliangunc/PIDD1-lissencephaly. Software used in this study: GATK 4.1 (https://www.broadinstitute.org/gatk); PLINK version 1.9 (http://pngu.mgh.harvard.edu/~purcell/plink); CADD version 1.6/ANNOVAR (http://annovar.openbioinformatics.org); Burrows-Wheeler Aligner tool (v0.7.15), Picard's MarkDuplicates, (v2.18.29), KING (v2.2.7), Picard (v2.25.6), SnpEff (v5.1), Ensembl Variant Effect Predictor (v107) , CellRanger (v6.1.2), R v4.3.0, Seurat version v4.3.0. Mass spec: Progenesis QI software (Nonlinear Dynamics, version 4.2), Bioconductor v3.18. GraphPad Prism version 10.3.1 was used for statistical analyses.

For manuscripts utilizing custom algorithms or software that are central to the research but not yet described in published literature, software must be made available to editors and reviewers. We strongly encourage code deposition in a community repository (e.g. GitHub). See the Nature Portfolio guidelines for submitting code & software for further information.

Data

Policy information about availability of data

All manuscripts must include a data availability statement. This statement should provide the following information, where applicable:

- Accession codes, unique identifiers, or web links for publicly available datasets
- A description of any restrictions on data availability
- For clinical datasets or third party data, please ensure that the statement adheres to our policy

Summary statistics for WES data analyses are provided in Supplementary Tables 1 and 3. Individual-level phenotype data of patients with PIDD1 mutations are provided in Supplementary Table 2. Sequencing data of patients with PIDD1 mutations are publicly restricted due to consent forms not allowing broad sharing of raw genomic data. Single-cell RNA-Seq files have been deposited in Sequence Read Archive (SRA) at Accession PRJNA1168541. Mass spectrometry data have been deposited in Proteomics Identification Database (PRIDE) at Accession PXD056364. Alphafold (https://alphafold.ebi.ac.uk/) was used to predict PIDD1 protein structure. Human Brain Transcriptome (HBT) (https://hbatlas.org/pages/hbtd) was used to display PIDD1 mRNA expression across brain regions and developmental time points. Pathway enrichment analysis was performed using the MSigDB_2020 gene set from GSEA (https://www.gsea-msigdb.org/gsea/index.jsp), OMIM dataset (www.omim.org), and Reactome 2022 pathway database (https://reactome.org/).

Human research participants

Policy information about studies involving human research participants and Sex and Gender in Research.

Reporting on sex and gender	Sex or gender had no impact on data; we generated an iPSC line from a female patient.
Population characteristics	The patient line was generated from a female recruited at age 11, and harbors a homozygous R331X PIDD1 mutation, diagnosed with diffuse pachygyria. The MDLS line was generated from a female sampled at age 1 per Coriell (https://www.coriell.org/0/sections/Search/Sample_Detail.aspx?Ref=GM26025&Product=CC) and harbors a heterozygous 46,XX,del(17)(p13.1p13.3)[25].arr[hg19] 17p13.3p13.2(513-4,242,178) genotype (https://www.coriell.org/0/sections/Search/Sample_Detail.aspx?Ref=GM26025&Product=CC), and was diagnosed with lissencephaly. The outside-family control iPSC lines were derived by the Yale Stem Cell Core from a healthy female subject at age 26. The patient, MDLS, and control iPSC lines were treated with and without NV-5138 (mTORC1 activator) for a subset of experiments reported in the study. The participants did not receive any treatment.
Recruitment	Participants were diagnosed with lissencephaly confirmed by imaging studies and were referred by treating physicians. No additional recruitment criteria were applied.
Ethics oversight	The study was approved by the Yale Human Investigations Committee (HIC protocol 9406007680). Institutional Review Board approvals for genetic and imaging studies, including written consent forms from all study subjects, were obtained by the referring physicians at the participating institutions.

Note that full information on the approval of the study protocol must also be provided in the manuscript.

Field-specific reporting

Please select the one below that is the best fit for your research. If you are not sure, read the appropriate sections before making your selection.

☒ Life sciences ☐ Behavioural & social sciences ☐ Ecological, evolutionary & environmental sciences

For a reference copy of the document with all sections, see nature.com/documents/nr-reporting-summary-flat.pdf

Life sciences study design

All studies must disclose on these points even when the disclosure is negative.

Sample size	No sample size calculation was performed. Previous studies have shown that in a well-established organoid protocol, batches and not individual organoids are the greatest source of variability (Camp et al. 2015, Kanton et al., 2019). A consistent phenotype was demonstrated when observed in a minimum of two independent batches. All organoid immunostaining experiments were performed with at least n=6 cortical regions, n=2 organoids, and n=2 independent batches. For proteomic analyses, n=3 biological replicates (each replicate with 3 organoids) were used per genotype. For scRNA-seq analyses, at least n=2 organoids/replicates were used for each genotype. For Figure 3:C, n=4; P, n=4; KI, n=2, PR, n=2. For Ext. Figure 8: n=2; C+NV, n=2; P, n=2, P+NV, n=2, MDLS, n=2, MDLS+NV, n=2. For western blot analyses, n=4 independent batches for p-S6/S6, n=3 independent batches for pAKT/AKT, 3 organoids harvested per batch per genotype
Data exclusions	Single-cells in scRNA-seq were excluded based on established quality control criteria prior to data collection; no data samples were excluded.
Replication	All quantifications were performed on a minimum of two independent organoid batches, with a minimum of 6 cortical regions per genotype. All attempts at replication were successful. For the full list of exact number of cortical regions analyzed, please see supplementary table 4.

Randomization	Organoids were transferred to culture dishes in a random order and by mixing organoids of the same genotype within the same batch.
Blinding	The investigators were not blinded during data collection and analysis, as most of the tissue collection, processing, and analyses were performed by one researcher.

Behavioural & social sciences study design

All studies must disclose on these points even when the disclosure is negative.

Study description	*Briefly describe the study type including whether data are quantitative, qualitative, or mixed-methods (e.g. qualitative cross-sectional, quantitative experimental, mixed-methods case study).*
Research sample	*State the research sample (e.g. Harvard university undergraduates, villagers in rural India) and provide relevant demographic information (e.g. age, sex) and indicate whether the sample is representative. Provide a rationale for the study sample chosen. For studies involving existing datasets, please describe the dataset and source.*
Sampling strategy	*Describe the sampling procedure (e.g. random, snowball, stratified, convenience). Describe the statistical methods that were used to predetermine sample size OR if no sample-size calculation was performed, describe how sample sizes were chosen and provide a rationale for why these sample sizes are sufficient. For qualitative data, please indicate whether data saturation was considered, and what criteria were used to decide that no further sampling was needed.*
Data collection	*Provide details about the data collection procedure, including the instruments or devices used to record the data (e.g. pen and paper, computer, eye tracker, video or audio equipment) whether anyone was present besides the participant(s) and the researcher, and whether the researcher was blind to experimental condition and/or the study hypothesis during data collection.*
Timing	*Indicate the start and stop dates of data collection. If there is a gap between collection periods, state the dates for each sample cohort.*
Data exclusions	*If no data were excluded from the analyses, state so OR if data were excluded, provide the exact number of exclusions and the rationale behind them, indicating whether exclusion criteria were pre-established.*
Non-participation	*State how many participants dropped out/declined participation and the reason(s) given OR provide response rate OR state that no participants dropped out/declined participation.*
Randomization	*If participants were not allocated into experimental groups, state so OR describe how participants were allocated to groups, and if allocation was not random, describe how covariates were controlled.*

Ecological, evolutionary & environmental sciences study design

All studies must disclose on these points even when the disclosure is negative.

Study description	*Briefly describe the study. For quantitative data include treatment factors and interactions, design structure (e.g. factorial, nested, hierarchical), nature and number of experimental units and replicates.*
Research sample	*Describe the research sample (e.g. a group of tagged Passer domesticus, all Stenocereus thurberi within Organ Pipe Cactus National Monument), and provide a rationale for the sample choice. When relevant, describe the organism taxa, source, sex, age range and any manipulations. State what population the sample is meant to represent when applicable. For studies involving existing datasets, describe the data and its source.*
Sampling strategy	*Note the sampling procedure. Describe the statistical methods that were used to predetermine sample size OR if no sample-size calculation was performed, describe how sample sizes were chosen and provide a rationale for why these sample sizes are sufficient.*
Data collection	*Describe the data collection procedure, including who recorded the data and how.*
Timing and spatial scale	*Indicate the start and stop dates of data collection, noting the frequency and periodicity of sampling and providing a rationale for these choices. If there is a gap between collection periods, state the dates for each sample cohort. Specify the spatial scale from which the data are taken*
Data exclusions	*If no data were excluded from the analyses, state so OR if data were excluded, describe the exclusions and the rationale behind them, indicating whether exclusion criteria were pre-established.*
Reproducibility	*Describe the measures taken to verify the reproducibility of experimental findings. For each experiment, note whether any attempts to repeat the experiment failed OR state that all attempts to repeat the experiment were successful.*
Randomization	*Describe how samples/organisms/participants were allocated into groups. If allocation was not random, describe how covariates were controlled. If this is not relevant to your study, explain why.*

Blinding

Describe the extent of blinding used during data acquisition and analysis. If blinding was not possible, describe why OR explain why blinding was not relevant to your study.

Did the study involve field work? ☐ Yes ☐ No

Field work, collection and transport

Field conditions

Describe the study conditions for field work, providing relevant parameters (e.g. temperature, rainfall).

Location

State the location of the sampling or experiment, providing relevant parameters (e.g. latitude and longitude, elevation, water depth).

Access & import/export

Describe the efforts you have made to access habitats and to collect and import/export your samples in a responsible manner and in compliance with local, national and international laws, noting any permits that were obtained (give the name of the issuing authority, the date of issue, and any identifying information).

Disturbance

Describe any disturbance caused by the study and how it was minimized.

Reporting for specific materials, systems and methods

We require information from authors about some types of materials, experimental systems and methods used in many studies. Here, indicate whether each material, system or method listed is relevant to your study. If you are not sure if a list item applies to your research, read the appropriate section before selecting a response.

Materials & experimental systems

n/a	Involved in the study
☐	☒ Antibodies
☐	☒ Eukaryotic cell lines
☒	☐ Palaeontology and archaeology
☒	☐ Animals and other organisms
☒	☐ Clinical data
☒	☐ Dual use research of concern

Methods

n/a	Involved in the study
☒	☐ ChIP-seq
☒	☐ Flow cytometry
☐	☒ MRI-based neuroimaging

Antibodies

Antibodies used

Primary antibodies (immunostaining)
mouse anti-MAP2 (1:500, MAB3418, Millipore)
mouse anti-SOX2 (1:500, sc-365823; Santa Cruz)
rat anti-SOX2 (1:500, 14-9811-82, Invitrogen)
rat anti-CTIP2 (1:500, ab18465; Abcam)
rabbit anti-SATB2 (1:500, ab34735, Abcam)
rabbit anti-TBR1 (1:500, ab31940, Abcam)
rabbit anti-HOPX (1:2500, HPA030180, Sigma)
mouse anti-HOPX (1:250, sc-398703, Santa Cruz)
rabbit anti-cleaved caspase 3 (1:1000, 9661, Cell Signaling Technologies)
mouse anti-PH3 (1:500, 9706, Cell Signaling Technologies)
mouse anti-Ki67 (1:500, 556003, BD Biosciences)
rabbit anti-EOMES (TBR2) (1:500, HPA028896, Sigma)
sheep anti-EOMES (TBR2) (1:200, AF6166, R&D)
rabbit anti-Phospho-S6 Ribosomal Protein (PS6) (1:200, 4858, Cell Signaling Technologies)

Secondary antibodies (immunostaining)
Alexa Flour 488 anti-sheep (1:1000, A11015, Thermofisher)
Alexa Fluor 488 ant-rat (1:1000, A21208, Thermofisher)
Alexa Fluor 568 anti-rabbit (1:1000, A10042, Thermofisher)
Alexa Fluor 647 anti-mouse (1:1000, A31571, Thermofisher)

Primary antibodies (western blotting)
mouse anti-PIDD1 (Anto-1) (1:500, ALX-804-837-C100, Enzo)
rabbit anti-PS6 (1:1000, 4858, Cell Signaling Technologies)
rabbit anti-S6 Ribosomal protein (5G10) (1:1000, 2217, Cell Signaling Technologies)
rabbit anti-Phospho-AKT (Ser473) (1:1000, 4060, Cell Signaling Technologies)
rabbit anti-Akt (pan) (C67E7), (1:1000, 4691, Cell Signaling Technologies)
mouse anti-beta-actin (1:5000, A2228, Sigma)

Secondary antibodies (western blotting)
anti-rabbit IgG, HRP (1:2000, 7074, Cell Signaling Technologies)
anti-mouse IgG, HRP (1:2000-5000, 7076, Cell Signaling Technologies)

Validation

Antibodies were chosen if reported to work on human tissue and in the method used (i.e., immunohistochemistry, western blot). Each antibody was validated based on previously published data listed on the manufacturer's website and antibody validation statement.
mouse anti-MAP2 (1:500, MAB3418, Millipore) is reactive to human and cited in 100 publications.
mouse anti-SOX2 (1:500, sc-365823; Santa Cruz) is reactive to human and cited in 300 publications.
rat anti-SOX2 (1:500, 14-9811-82, Invitrogen) is reactive to human and cited in 67 publications.
rat anti-CTIP2 (1:500, ab18465; Abcam) is reactive to human and cited in 841 publications.
rabbit anti-SATB2 (1:500, ab34735, Abcam is reactive to human and cited in 90 publications.
rabbit anti-TBR1 (1:500, ab31940, Abcam is reactive to human and cited in 476 publications.
rabbit anti-HOPX (1:2500, HPA030180, Sigma) is reactive to human and cited in 31 publications.
mouse anti-HOPX (1:250, sc-398703, Santa-Cruz) is reactive to human and cited in 82 publications.
rabbit anti-cleaved caspase 3 (1:1000, 9661, Cell Signaling Technologies) is reactive to human and cited in 10478 publications.
mouse anti-PIDD1 (Anto-1) (1:500, ALX-804-837-C100, Enzo) is reactive to human and cited in 4 publications.
rabbit anti-PS6 (1:1000, 4858, Cell Signaling Technologies) is reactive to human and cited in 1590 publications.
rabbit anti-S6 Ribosomal protein (5G10) (1:1000, 2217, Cell Signaling Technologies) is reactive to human and cited in 2378 publications.
rabbit anti-Phospho-AKT (Ser473) (1:1000, 4060, Cell Signaling Technologies) is reactive to human and cited in 7877 publications.
rabbit anti-Akt (pan) (C67E7), (1:1000, 4691, Cell Signaling Technologies) is reactive to human and cited in 5474 publications.
mouse anti-beta-actin (1:5000, A2228, Sigma) is reactive to human and cited in 2979 publications.
mouse anti-PH3 (1:500, 9706, Cell Signaling Technologies) is reactive to human and cited in 473 publications.
mouse anti-Ki67 (1:500, 556003, BD Biosciences) is reactive to human and cited in 299 publications.
rabbit anti-EOMES (TBR2) (1:500, HPA028896, Sigma) is reactive to human and cited in 4 publications.
sheep anti-EOMES (TBR2) (1:200, AF6166, R&D) is reactive to human and cited in 25 publications.
rabbit anti-Phospho-S6 Ribosomal Protein (PS6) (1:200, 4858, Cell Signaling Technologies) is reactive to human and cited in 1590 publications.

Manufacturer company validation statements/protocols:
Abcam: https://www.abcam.com/primary-antibodies/how-we-validate-our-antibodies
BD Biosciences: https://www.bdbiosciences.com/en-us/products/reagents/flow-cytometry-reagents/research-reagents/quality-and-reproducibility
Cell Signaling Technologies: https://www.cellsignal.com/about-us/cst-antibody-validation-principles
Enzo: https://www.enzolifesciences.com/ALX-804-837/pidd-monoclonal-antibody-anto-1
Milipore: https://www.emdmillipore.com/US/en/life-science-research/antibodies-assays/antibodies-overview/Antibody-Development-and-Validation/cFOb.qB.8McAAAFOb64qQvSS,nav
Santa Cruz: https://www.scbt.com/resources/protocols/immunofluorescence-cell-staining
Sigma: https://www.sigmaaldrich.com/US/en/products/protein-biology/antibodies/prestige-antibodies
Thermofisher: https://www.thermofisher.com/us/en/home/life-science/antibodies/invitrogen-antibody-validation.html
Sigma (mouse beta actin): https://www.sigmaaldrich.com/US/en/technical-documents/technical-article/protein-biology/elisa/antibody-standard-validation

Eukaryotic cell lines

Policy information about cell lines and Sex and Gender in Research

Cell line source(s)

MDLS iPSCs (Coriell Repository, GM26025); Patient iPSCs (derived in-house from patient hair follicle keratinocytes), and Control iPSCs (derived in-house at the Yale Stem Cell Core). The Knock-In (KI) line was derived via CRISPR-Cas9 gene editing in-house from the Control line. The Patient Rescue (PR) line was derived via CRISPR-Cas9 gene editing in-house from the Patient line.

Authentication

MDLS iPSCs were obtained from Coriell (catalog # GM26025) and authenticated using Agilent 60k Standard microarray comparative genomic hybridization and karyotyping performed by Cell LIne Genetics (Ext. Data Fig .3). Control iPSC line was obtained from the Yale School of Medicine Stem Cell Core and authenticated through karyotyping, teratoma assay, and Sanger sequencing confirming no R331X mutation (Ext. Data Fig. 3). The Patient line was generated using the CytoTune 2.0 Sendai virus kit and authenticated by karyotyping, pluripotency marker staining, and Sanger sequencing confirming the homozygous R331X mutation (Ext. Data Fig 3). The Patient Rescue and Knock-In lines were authenticated by karyotyping and Sanger sequencing confirming the intended edit (WT/WT and R331X/R331X) respectively (Ext. Data Fig. 3).

Mycoplasma contamination

iPSC lines were tested and found to be negative for mycoplasma contamination.

Commonly misidentified lines
(See ICLAC register)

No commonly misidentified lines was used in the study.

Palaeontology and Archaeology

Specimen provenance

Provide provenance information for specimens and describe permits that were obtained for the work (including the name of the issuing authority, the date of issue, and any identifying information). Permits should encompass collection and, where applicable, export.

Specimen deposition	*Indicate where the specimens have been deposited to permit free access by other researchers.*
Dating methods	*If new dates are provided, describe how they were obtained (e.g. collection, storage, sample pretreatment and measurement), where they were obtained (i.e. lab name), the calibration program and the protocol for quality assurance OR state that no new dates are provided.*

☐ Tick this box to confirm that the raw and calibrated dates are available in the paper or in Supplementary Information.

Ethics oversight	*Identify the organization(s) that approved or provided guidance on the study protocol, OR state that no ethical approval or guidance was required and explain why not.*

Note that full information on the approval of the study protocol must also be provided in the manuscript.

Animals and other research organisms

Policy information about studies involving animals; ARRIVE guidelines recommended for reporting animal research, and Sex and Gender in Research

Laboratory animals	*For laboratory animals, report species, strain and age OR state that the study did not involve laboratory animals.*
Wild animals	*Provide details on animals observed in or captured in the field; report species and age where possible. Describe how animals were caught and transported and what happened to captive animals after the study (if killed, explain why and describe method; if released, say where and when) OR state that the study did not involve wild animals.*
Reporting on sex	*Indicate if findings apply to only one sex; describe whether sex was considered in study design, methods used for assigning sex. Provide data disaggregated for sex where this information has been collected in the source data as appropriate; provide overall numbers in this Reporting Summary. Please state if this information has not been collected. Report sex-based analyses where performed, justify reasons for lack of sex-based analysis.*
Field-collected samples	*For laboratory work with field-collected samples, describe all relevant parameters such as housing, maintenance, temperature, photoperiod and end-of-experiment protocol OR state that the study did not involve samples collected from the field.*
Ethics oversight	*Identify the organization(s) that approved or provided guidance on the study protocol, OR state that no ethical approval or guidance was required and explain why not.*

Note that full information on the approval of the study protocol must also be provided in the manuscript.

Clinical data

Policy information about clinical studies

All manuscripts should comply with the ICMJE guidelines for publication of clinical research and a completed CONSORT checklist must be included with all submissions.

Clinical trial registration	*Provide the trial registration number from ClinicalTrials.gov or an equivalent agency.*
Study protocol	*Note where the full trial protocol can be accessed OR if not available, explain why.*
Data collection	*Describe the settings and locales of data collection, noting the time periods of recruitment and data collection.*
Outcomes	*Describe how you pre-defined primary and secondary outcome measures and how you assessed these measures.*

Dual use research of concern

Policy information about dual use research of concern

Hazards

Could the accidental, deliberate or reckless misuse of agents or technologies generated in the work, or the application of information presented in the manuscript, pose a threat to:

No	Yes	
☐	☐	Public health
☐	☐	National security
☐	☐	Crops and/or livestock
☐	☐	Ecosystems
☐	☐	Any other significant area

Experiments of concern

Does the work involve any of these experiments of concern:

No	Yes	
☐	☐	Demonstrate how to render a vaccine ineffective
☐	☐	Confer resistance to therapeutically useful antibiotics or antiviral agents
☐	☐	Enhance the virulence of a pathogen or render a nonpathogen virulent
☐	☐	Increase transmissibility of a pathogen
☐	☐	Alter the host range of a pathogen
☐	☐	Enable evasion of diagnostic/detection modalities
☐	☐	Enable the weaponization of a biological agent or toxin
☐	☐	Any other potentially harmful combination of experiments and agents

ChIP-seq

Data deposition

☐ Confirm that both raw and final processed data have been deposited in a public database such as GEO.

☐ Confirm that you have deposited or provided access to graph files (e.g. BED files) for the called peaks.

Data access links *May remain private before publication.*	*For "Initial submission" or "Revised version" documents, provide reviewer access links. For your "Final submission" document, provide a link to the deposited data.*
Files in database submission	*Provide a list of all files available in the database submission.*
Genome browser session (e.g. UCSC)	*Provide a link to an anonymized genome browser session for "Initial submission" and "Revised version" documents only, to enable peer review. Write "no longer applicable" for "Final submission" documents.*

Methodology

Replicates	*Describe the experimental replicates, specifying number, type and replicate agreement.*
Sequencing depth	*Describe the sequencing depth for each experiment, providing the total number of reads, uniquely mapped reads, length of reads and whether they were paired- or single-end.*
Antibodies	*Describe the antibodies used for the ChIP-seq experiments; as applicable, provide supplier name, catalog number, clone name, and lot number.*
Peak calling parameters	*Specify the command line program and parameters used for read mapping and peak calling, including the ChIP, control and index files used.*
Data quality	*Describe the methods used to ensure data quality in full detail, including how many peaks are at FDR 5% and above 5-fold enrichment.*
Software	*Describe the software used to collect and analyze the ChIP-seq data. For custom code that has been deposited into a community repository, provide accession details.*

Flow Cytometry

Plots

Confirm that:

☐ The axis labels state the marker and fluorochrome used (e.g. CD4-FITC).

☐ The axis scales are clearly visible. Include numbers along axes only for bottom left plot of group (a 'group' is an analysis of identical markers).

☐ All plots are contour plots with outliers or pseudocolor plots.

☐ A numerical value for number of cells or percentage (with statistics) is provided.

Methodology

Sample preparation	*Describe the sample preparation, detailing the biological source of the cells and any tissue processing steps used.*
Instrument	*Identify the instrument used for data collection, specifying make and model number.*

Software

Describe the software used to collect and analyze the flow cytometry data. For custom code that has been deposited into a community repository, provide accession details.

Cell population abundance

Describe the abundance of the relevant cell populations within post-sort fractions, providing details on the purity of the samples and how it was determined.

Gating strategy

Describe the gating strategy used for all relevant experiments, specifying the preliminary FSC/SSC gates of the starting cell population, indicating where boundaries between "positive" and "negative" staining cell populations are defined.

☐ Tick this box to confirm that a figure exemplifying the gating strategy is provided in the Supplementary Information.

Magnetic resonance imaging

Experimental design

Design type

Lissencephaly diagnosis was confirmed by at least one imaging study (Magnetic Resonance Imaging) in all index cases and family members. All available imaging for study participants who underwent whole-exome sequencing were obtained and reviewed by a minimum of two clinicians (attending neuroradiologists).

Design specifications

Available brain MRI scans were reviewed for lissencephaly/pachygyria.

Behavioral performance measures

N/A

Acquisition

Imaging type(s)

Structural

Field strength

1.5T - 3T

Sequence & imaging parameters

Clinical imaging protocols varied depending on institution, but were within the "standard" for structural MRI brain scans. Sequences evaluated included T1-weighted, T2-weighted, and T2-FLAIR.

Area of acquisition

Entire brain

Diffusion MRI ☐ Used ☒ Not used

Preprocessing

Preprocessing software

Processing was performed by the clinical institution

Normalization

Processing was performed by the clinical institution

Normalization template

Processing was performed by the clinical institution

Noise and artifact removal

Processing was performed by the clinical institution

Volume censoring

Processing was performed by the clinical institution

Statistical modeling & inference

Model type and settings

No statistical modeling was performed.

Effect(s) tested

N/A

Specify type of analysis: ☐ Whole brain ☐ ROI-based ☐ Both

Statistic type for inference (See Eklund et al. 2016)

N/A

Correction

N/A

Models & analysis

n/a	Involved in the study
☒	☐ Functional and/or effective connectivity
☒	☐ Graph analysis
☒	☐ Multivariate modeling or predictive analysis

Functional and/or effective connectivity

Report the measures of dependence used and the model details (e.g. Pearson correlation, partial correlation,

Functional and/or effective connectivity	*mutual information).*
Graph analysis	*Report the dependent variable and connectivity measure, specifying weighted graph or binarized graph, subject- or group-level, and the global and/or node summaries used (e.g. clustering coefficient, efficiency, etc.).*
Multivariate modeling and predictive analysis	*Specify independent variables, features extraction and dimension reduction, model, training and evaluation metrics.*